Molecular Therapy
Methods & Clinical Development
Original Article

A Novel Proteomic Method Reveals NLS Tagging of T-DM1 Contravenes Classical Nuclear Transport in a Model of HER2-Positive Breast Cancer

Vincent Lacasse,[1] Simon Beaudoin,[1] Steve Jean,[2] and Jeffrey V. Leyton[1,3]

[1]Department of Nuclear Medicine and Radiobiology, Faculty of Medicine and Health Sciences, Centre Hospitalier Universitaire de Sherbrooke (CHUS), Université de Sherbrooke (UdeS), Sherbrooke, QC J1H 5N4, Canada; [2]Department of Immunology and Cell Biology, Faculty of Medicine and Health Sciences, CHUS, UdeS, Sherbrooke, QC J1H 5N4, Canada; [3]Sherbrooke Molecular Imaging Centre (CIMS), Centre de Recherche du CHUS, UdeS, Sherbrooke, QC J1H 5N4, Canada

The next breakthrough for protein therapeutics is effective intracellular delivery and accumulation within target cells. Nuclear localization signal (NLS)-tagged therapeutics have been hindered by the lack of efficient nuclear localization due to endosome entrapment. Although development of strategies for tagging therapeutics with technologies capable of increased membrane penetration has resulted in proportional increased potency, nonspecific membrane penetration limits target specificity and, hence, widespread clinical success. There is a long-standing idea that nuclear localization of NLS-tagged agents occurs exclusively via classical nuclear transport. In the present study, we modified the antibody-drug conjugate trastuzumab-emtansine (T-DM1) with a classical NLS linked to cholic acid (cell accumulator [Accum]) that enables modified antibodies to escape endosome entrapment and increase nuclear localization efficiency without abrogating receptor targeting. In parallel, we developed a proteomics-based method to evaluate nuclear transport. Accum-modified T-DM1 significantly enhanced cytotoxic efficacy in the human epidermal growth factor receptor 2 (HER2)-positive SKBR3 breast cancer system. We discovered that efficacy was dependent on the nonclassical importin-7. Our evaluation reveals that when multiple classical NLS tagging occurs, cationic charge build-up as opposed to sequence dominates and becomes a substrate for importin-7. This study results in an effective target cell-specific NLS therapeutic and a general approach to guide future NLS-based development initiatives.

INTRODUCTION

At a glance, the enormous research development and the increasing availability of biopharmaceuticals make it appear that these precision-targeted drugs will make good on their promise to provide more effective treatments for disease.[1] However, many novel anticancer biopharmaceuticals are perceived as providing insufficient benefits, and because they are expensive, their cost-effectiveness has been questioned.[2,3] Two major challenges limiting the full effectiveness of biopharmaceuticals are (1) the inability of large biological molecules to cross the plasma membrane while retaining target cell specificity, and (2) the need to improve the intracellular accumulation of biopharmaceuticals transporting payloads to sufficient levels to evoke an effective cellular response for the given therapeutic application. These barriers must be improved for next-generation biopharmaceuticals, yet insights and accompanying enhancing technologies are yet to be fully realized.

Signal peptides are an integral component of intracellular protein targeting. The application of nuclear localization signal (NLS) tagging for non-viral transfer of oligonucleotides, proteins, and reporter molecules is being widely investigated for the development of therapeutic medicines. For example, nuclear targeting via NLS tagging is improving efficient localization of DNA vaccines into the cell nucleus for subsequent expression of immunogenic peptides, which is a constant concern for clinical success.[4] Nuclear targeting of theranostic radionuclides is being implemented in the clinic to apply short-range-emitting radionuclides to impart high ionization densities at the site of decay, which maximizes DNA damage and could overcome much of the toxicity with traditional radiation approaches.[5] Among nanotechnology-based therapies, whose primary benefits are improved intracellular delivery of encapsulated drugs for reduced dosing, are actively being NLS tagged to improve intracellular targeting.[6] Hence, NLS-tagged agents are critical for future effective medicines. Unfortunately, the barriers of NLS-tagged agents include target cell binding, internalization, and endosomal escape, resulting in poor nuclear localization efficiency.[7]

Since the discovery of the cell-penetrating peptides (CPPs),[8] three decades of significant research have elucidated the properties of membrane penetration and, more importantly, the ability of conjugation to biopharmaceuticals to deliver proteins specific for intracellular targets or to improve the delivery of cytotoxic payloads against a variety of diseases.[9] While CPP-tagged therapeutics can improve cell

Received 19 October 2019; accepted 27 August 2020;
https://doi.org/10.1016/j.omtm.2020.08.016.

Correspondence: Jeffrey V. Leyton, Department of Nuclear Medicine and Radiobiology, Faculty of Medicine and Health Sciences, Centre Hospitalier Universitaire de Sherbrooke (CHUS), Université de Sherbrooke (UdeS), Sherbrooke, QC J1H 5N4, Canada.
E-mail: jeffrey.leyton@usherbrooke.ca

membrane penetration, they lack specificity. Due to exquisite affinity and specificity of monoclonal antibodies (mAbs), attempts have been made to develop CPP-mAb conjugates to deliver payloads with high intracellular accumulation efficiency to target tumor cells. However, endosome entrapment continues to be a challenge.[10–12] In addition, the limitation of tissue and cellular specificity continues to plague CPP-tagged biopharmaceuticals.[13,14] To date, CPP-based drugs have reached the clinic in children and adults with glioblastoma (ClinicalTrials.gov: NCT01975116 and NCT00914914). Although they are well tolerated, reductions in tumor growth were marginal.[15]

In our previous work, we developed a short 13-aa peptide CGYGPKKKRKVGG containing the classical NLS (cNLS) from simian virus 40 (SV40) large T antigen (underlined) linked to a cholic acid (herein termed cell accumulator [Accum]) that addressed the current limitation with CPP- and NLS-tagged agents.[16] Accum-modified mAbs were able to traverse membranes only after being entrapped inside endosomes and were a requirement for efficient transport to and accumulation inside the nucleus of target cells.[16,17] The rationale for cholic acid stems from work demonstrating that bile acids are critical for triggering the enzyme acid sphingomyelinase to cleave sphingomyelin, which is abundantly present on the inner leaflet of endosomes, to form ceramide.[18,19] Increased amounts of ceramide destabilize membranes by forming channels or lipid flip-flop sufficient for proteins to cross.[20,21] Importantly, ceramide formation in endosome membranes facilitates viral escape without killing cells.[19] Therefore, we hypothesized that attaching cholic acid to an NLS peptide would enable mAbs to efficiently localize in the nucleus, without abrogating target cell specificity. Indeed, Accum-modified mAbs conjugated to radionuclides retained high target receptor affinity and specificity at the cell surface. Once internalized via receptor-mediated endocytosis, the coupled endosome escape-nuclear transport function of Accum enables efficient accumulation of the delivered antibody conjugate relative to unmodified mAbs and mAbs modified with the NLS but no cholic acid.[16,22] *In vivo*, Accum-modified mAbs targeted tumors with superior tumor cell accumulation and specificity of delivered radionuclides compared to non-Accum-modified counterparts.[17] Thus, Accum's effective intracellular transport system did not interfere with mAb targeting of receptors on tumor cells and was able to increase mAb (and payload) access to and accumulation in the nucleus of tumor cells, which improved tumor targeting.

Nuclear transport receptors (NTRs), also known as importins, mediate the transport of macromolecules across the nuclear pore complex.[23,24] Because NTRs have this unique capability, they are essential regulators for many normal cellular functions. The cNLS sequence PKKKRKV from the SV40 large T antigen was the sequence identified and used to elucidate nuclear transport more than three decades ago.[25–28] These studies revealed that proteins requiring entry into the nucleus contain an NLS that is recognized and bound by the adaptor protein importin-α. Importin-β then binds importin-α, and the complex is subsequently transported along the cytoskeleton by motor proteins and dock at the nuclear pore complex. The cargo is released into the nucleus through the binding of Ran-guanosine triphosphate (GTP). As a result, there has been a large effort by the research community to develop therapeutic agents for targeting proteins against intracellular structures to deliver molecular payloads, including gene therapy, tagged with the cNLS, as noted in several reviews on this topic.[29–34] However, there are >20 NTRs in the human genome, and most of the nuclear transport is performed by NTRs able to directly bind cargos in the absence of importin-α.[35] Whereas hundreds of cargos have been demonstrated or suggested for importin-α/β, only a limited number of substrates are known for most non-classical NTRs.[36] Moreover, there is even less knowledge on the nuclear transport systems with NLS-tagged therapeutics.

This study originated from our pondering whether NLS-tagged agents have been overly reliant on the cNLS and import mechanics and why these drugs have yet to be fully realized in the clinic. Major challenges blocking elucidation are that unique classes of NLS sequences of particular NTRs have not been identified and that NTRs share similar molecular weights, isoelectric points, and have low sequence identity.[35] In addition, cargos for most NTRs have been identified through binary protein-protein interaction assays.[37–39]

In the present study, we hypothesized whether Accum's unique delivery mechanism could be applied as a therapeutic agent. As a proof of concept, we examined the effect of incubating human epidermal growth factor receptor 2 (HER2)-positive SKBR3 cells with the clinically approved biopharmaceutical trastuzumab (Tmab)-emtansine (T-DM1) modified with Accum (herein Accum-T-DM1). Our rationale for using T-DM1 is that although T-DM1 stunts growth of tumors in breast cancer patients, many patients still experience disease progression.[40] One major implicated resistance factor is the incomplete trafficking of T-DM1 to the lysosome[41] and/or an inherent or acquired ability to recycle back to the plasma membrane.[42] This results in the inability of T-DM1 to accumulate sufficiently to effectively kill tumor cells. Although microtubules, the target of DM1, are present in the cytosol, Oroudjev et al.[43] showed that breast cancer cells in the prometaphase/metaphase rather than the interphase were more sensitive to antibody-DM1 conjugates. In addition, HER2 is well known to have limited internalization in SKBR3 cells.[42,44,45] Thus, with Accum-mediated nuclear transport and the importance of the nucleus on DM1 cytotoxicity, Accum-T-DM1 using the SKBR3 cell model could feasibly test our hypothesis.

We obtained clinical-grade T-DM1, modified it with Accum, and evaluated it for its ability to maintain overall complex stability and to determine whether it could localize in the nucleus and whether this delivery system enhanced cytotoxicity in the HER2-positive breast cancer cell line SKBR3. We also set out to address intracellular transport, as NLS-tagged pharmaceuticals continue to operate on the assumption that nuclear transport is, in general, mediated via the classical importin-α/importin-β complex. In addition, to our knowledge, there has never been an unbiased investigation on intracellular transport of CPP- or NLS-tagged agents. Hence, a pull-down assay was developed involving treatment of SKBR3 cells incubated with Accum-T-DM1, T-DM1, or Tmab followed by high-performance liquid

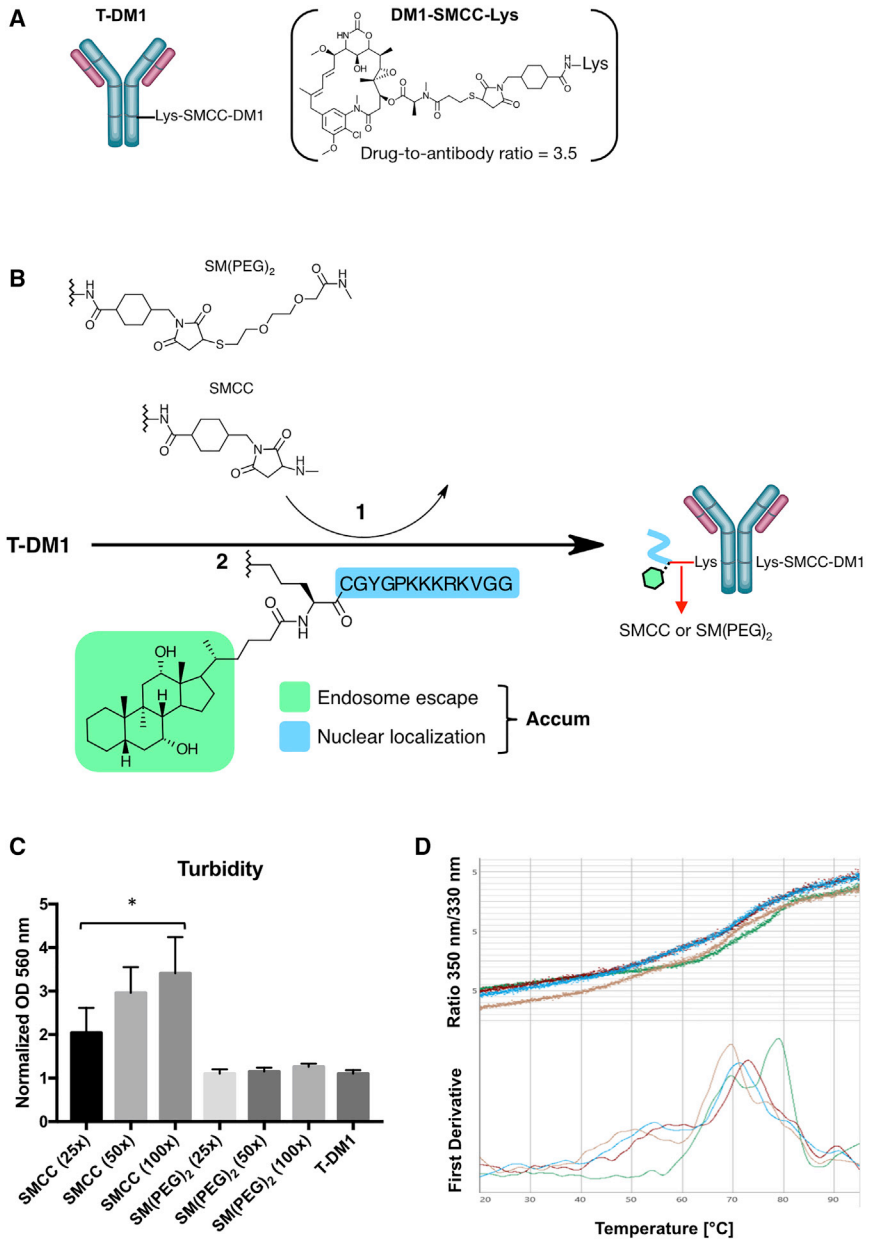

Figure 1. Accum Modification of T-DM1

Schematic representation of (A) trastuzumab-emtansine (T-DM1) and its major cytotoxic metabolite DM1-SMCC-lysine, and (B) Accum-T-DM1 construction depicted by steps (1) reaction of T-DM1 with SMCC or $SM(PEG)_2$ to yield maleimide-activated versions of T-DM1 and (2) subsequent Accum conjugation to yield versions of Accum-modified T-DM1. (C) Turbidity assay of Accum-T-DM1 using increasing SMCC- or $SM(PEG)_2$-to-T-DM1 ratios (*$p < 0.0001$). (D) Differential scanning fluorimetry thermograms of T-DM1 (green), Acc_L-T-DM1 (red), Acc_M-T-DM1 (blue), and Acc_H-T-DM1 (orange) made with $SM(PEG)_2$. Top: the 350 nm/330 nm fluorescence ratio versus temperature gradient. Bottom: the corresponding first derivatives are shown.

chromatography- tandem mass spectrometry (HPLC-MS/MS). We organized our proteomic data into two different but complementary bait-prey systems to extract proteins with the highest confidence that specifically interact only with the Accum portion of Accum-T-DM1. We then conducted cytotoxicity assays in SKBR3 cells depleted of identified NTRs. Our findings showed that Accum-T-DM1 could be constructed as an NLS-modified agent and that it increased cytotoxicity by several-fold relative to T-DM1 and was specific for HER2. Tagging T-DM1 with NLS only (no cholic acid) or Tmab with Accum did not increase cytotoxic impact. This indicated that Accum-enabled endosome escape and nuclear localization were the essential factors for increasing the cytotoxic effectiveness of T-DM1. Importantly, our findings showed that Accum-T-DM1 was not reliant on the classical NTR complex for enhanced cytotoxicity in the SKBR3 cell model. In contrast, Accum-T-DM1 nuclear localization and cytotoxicity were reliant on the non-classical NTR importin-7 (IPO7). A recently available cryogenic electron microscopy (cryo-EM) structure of IPO7 in complex with importin-β1 (KPNB1) and histone H1 revealed that IPO7 utilizes cation interactions to recognize and bind to cargo proteins. Analysis of the IPO7 binding pocket provides suggestive mechanistic evidence for why Accum-modified T-DM1 is preferentially reliant on IPO7 and not importin-α. Accum combined with our proteomic and biochemical methods result in a potentially readily available approach and an evaluative guide on nuclear transport pathways for future NLS-based therapeutics.

RESULTS

Molecular Basis of Accum Conjugation to T-DM1 for Stability, Activity, and Proteomic Processing

T-DM1 contains a DM1-to-antibody ratio value of 3.5 that uses the crosslinker succinimidyl-4-(*N*-maleimidomethyl)cyclohexane-1-carboxylate (SMCC) to conjugate DM1 to surface lysines present on Tmab (Figure 1A).[46,47] A widely used method for peptide conjugation onto mAbs is via the attachment to surface lysines. Although modification with dyes on surface lysines of T-DM1 have previously been performed without affecting activity,[48] it was unknown how peptide crosslinking would affect T-DM1 stability, function, and downstream use as the proteomic bait. The cytotoxin DM1 is hydrophobic, and the effect of modifying Tmab, first to form the intermediate Tmab crosslinker, then to form the full T-DM1, promotes aggregation.[47] Thus, we evaluated two crosslinker types for the conjugation of Accum to Tmab surface lysines. T-DM1 was maleimide-activated by reacting it with 25-, 50-,

and 100-fold molar excess SMCC or polyethylene glycol (PEG)ylated SMCC ($SM(PEG)_2$) (Figure 1B). The intermediate species was then purified and reacted with Accum that contains an N-terminal cysteine that reacts with $SM(PEG)_2$ or SMCC and forms Accum-T-DM1 (Figure 1B).

As a first analysis method, a turbidity assay in combination with SDS-PAGE was used to evaluate stability. Accum-T-DM1 modified using all tested excess ratios of $SM(PEG)_2$ showed no increased aggregation relative to T-DM1. In contrast, aggregation was increased up to 3-fold when the SMCC-based conjugation was used (Figure 1C). SDS-PAGE analysis also confirmed that the SMCC-based Accum-T-DM1 conjugates were highly aggregated (Figure S1A). The primary evidence by SDS-PAGE was the diminished band intensity for the different Accum-T-DM1 versions indicating the absence of soluble protein. In contrast, using $SM(PEG)_2$ showed no increased aggregation relative to unmodified T-DM1 (Figure 1C). In addition, SDS-PAGE showed the clear migration of both the light chain (LC) and heavy chain (HC) with increased molecular weights in Accum-$SM(PEG)_2$-T-DM1 constructs relative to T-DM1 (Figure S1B). The Accum-modified T-DM1 conjugates were >90% monomers when 25- and 50-fold excess $SM(PEG)_2$ crosslinker ratios were utilized. Only Accum-modified T-DM1 with 100-fold excess $SM(PEG)_2$ crosslinker showed that there was aggregation present, again due to diminished band intensity (Figure S1B). Thus, the PEG-based crosslinker and its increased water solubility relative to SMCC provided a successful conjugation approach to produce highly soluble versions of Accum-T-DM1 conjugates. Herein, the Accum loads for T-DM1 modified with 25-, 50-, and 100-fold excess $SM(PEG)_2$ are termed AccumLow (Acc_L), AccumMedium (Acc_M), and AccumHigh (Acc_H), respectively.

Aggregation was further evaluated by label-free differential scanning fluorimetry (nanoDSF). Analyzing antibody-drug conjugate (ADC) stability with nanoDSF has proven effective for its ability to evaluate aggregation through the measurement of unfolding events of the mAb Fab, C_H2, and C_H3 domains.[49,50] T-DM1 and Acc_L-T-DM1 and Acc_M-T-DM1, but not Acc_H-T-DM1, exhibited comparable starting levels in the initial ratio (350 nm/330 nm) (Figure 1D). The thermal-induced unfolding transitions for T-DM1 C_H2 and C_H3 domains of the Fc region were 70.1°C ± 0.2°C and 79.5°C ± 0.4°C, respectively. In contrast, there was only a single unfolding transition for all Accum-T-DM1 conjugates. Acc_M-T-DM1 and Acc_H-T-DM1 ADCs had transitions at 70.4°C ± 1.3°C and 69.4°C ± 0.3°C, respectively. Acc_L-T-DM1 had an unfolding transition at 73.5°C ± 0.6°C. These transition temperatures correspond to the unfolding of the C_H2 domain. These results indicated an inverse correlation where increasing the number of $SM(PEG)_2$-activated lysines with subsequent Accum conjugation reduced the temperature values for the C_H2 unfolding transitions proportionally. This suggests that Accum modification has a greater impact on the C_H2 domain compared to other domains of T-DM1. Previous ADCs based on a human immunoglobulin G (IgG) conjugated via lysines to DM1 also showed that the C_H2 domain, relative to other domains, is the most likely to be destabilized due to a preference for DM1-lysine conjugations for C_H2.[50] Hence, the lysines used for Accum conjugation are most likely present in the C_H2 domain. Based on theses results, Accum-T-DM1 conjugates using $SM(PEG)_2$ were soluble and had stabilities sufficient for moving forward to functional evaluations in live cells.

Accum-T-DM1 Localizes to the Nucleus

Accum-modified T-DM1 localized to the nucleus whereas T-DM1 did not. Confocal microscopy images showed that T-DM1 was exclusively localized at or near (subcellular) the plasma membrane (Figure 2). These results are consistent with the known poor HER2 internalization kinetics caused by rapid recycling in SKBR3 cells.[42,44,45] T-DM1 in the cytosol of SKBR3 cells could not be readily visualized throughout this evaluation but suggests, nonetheless, that the amount of T-DM1 internalized and processed in the lysosome is still sufficient to cause cytotoxicity and was previously justified in the early development studies of T-DM1.[51,52]

In contrast, confocal microscopy images showed that at 0.5 h Acc_L-T-DM1 was internalized and distributed in the cytoplasm, shown as punctate foci typical of endosome entrapment. At 1 h Acc_L-T-DM1 was increasingly diffused throughout the cytoplasm. At 2 h, the immunofluorescence signal pertaining to Acc_L-T-DM1 was localized in the nucleus while still being abundantly present in the cytoplasm. This was consistent with Accum-modified antibodies that have previously targeted leukemia and invasive bladder cancer cells.[16,17] After 2 h, the signal in the nucleus gradually decreased, indicating protease degradation and DM1 release in the nucleus. This study demonstrates that Accum mediates a highly linear mode of delivering T-DM1 to the nucleus starting at endosome escape and nuclear transport, and finishing with release and accumulation inside the nucleus. More important for this study, the evidence suggests potential engagement of NTRs via NLS recognition and binding necessary for localization into the nucleus.

Accum Enhances T-DM1 Cytotoxicity

Only Accum modification enhanced T-DM1 cytotoxic potency. In addition, Accum modification did not abrogate HER2 target specificity for T-DM1. SKBR3 cells were chosen for this proof of concept because they are sensitive to T-DM1 but are known to have poor HER2 internalization processing to the lysosome due to rapid recycling back to the cell surface.[42] Since Accum has previously demonstrated the ability to escape internalized endosomes,[17] SKBR3 cells are ideal to evaluate the endosome escape-nuclear transport impact on cytotoxicity and whether it is enhanced relative to T-DM1. SKBR3 cells treated with T-DM1 resulted in a half-maximal inhibitory concentration (IC_{50}) value of 0.033 μg/mL (R^2 = 0.96). This result is among the IC_{50} values previously reported.[52,53] In contrast, SKBR3 cells treated with Acc_L-T-DM1, Acc_M-T-DM1, and Acc_H-T-DM1 resulted in IC_{50} values of 0.0036 μg/mL (R^2 = 0.95), 0.0029 μg/mL (R^2 = 0.99), and 0.0018 μg/mL (R^2 = 0.99), respectively (Figure 3A). To demonstrate specificity, cytotoxicity was evaluated in MCF-7 cells that have extremely low HER2 expression levels, comparable to normal cell HER2 expression.[54,55] No increased cytotoxicity

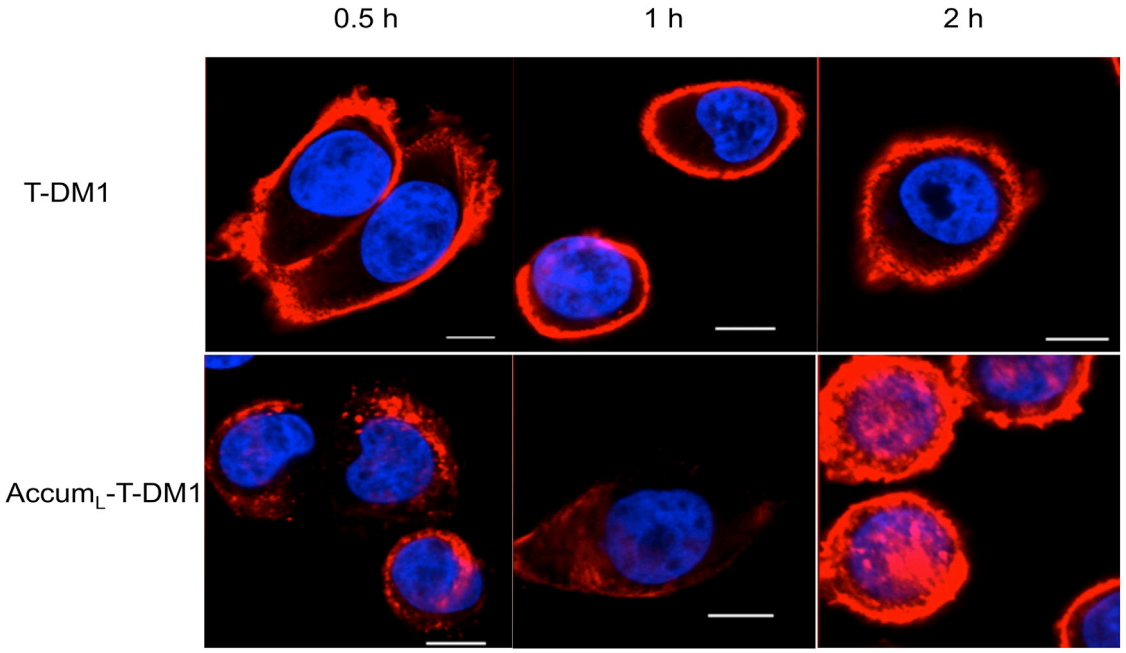

Figure 2. Immunofluorescence Confocal Microscopy Images Show Distribution of T-DM1 and Acc$_L$-T-DM1 in SKBR3 Cells at Various Time Points
Red depicts the antibody portion of either T-DM1 or Acc$_L$-T-DM1, and blue is the nucleus stained by Hoechst. Scale bars, 100 nm. Experiments were performed in triplicate.

against MCF-7 cells was observed due to the modification of T-DM1 with high Accum loading (Figure 3B).

To demonstrate that cholic acid-mediated endosome escape was essential, we evaluated T-DM1 modified with NLS alone (no cholic acid) in SKBR3 cells (Figure 3C). NLS was loaded onto T-DM1 in low (NLS$_L$), medium (NLS$_M$), and high (NLS$_H$) amounts, as was performed for Accum loading. NLS$_L$-T-DM1, NLS$_M$-T-DM1, and NLS$_H$-T-DM1 had IC_{50} values of 0.0186 μg/mL (R^2 = 0.93), 0.0092 μg/mL (R^2 = 0.8538), and 0.0057 μg/mL (R^2 = 0.8572), respectively. The NLS$_L$-modified T-DM1 construct had weaker cytotoxic potency compared to Acc$_L$-modified T-DM1 by a factor of 5.2. The NLS$_M$-T-DM1 and NLS$_H$-T-DM1 constructs had weaker cytotoxic potency compared to the Accum-modified T-DM1 counterparts by a factor of 3.2. This indicated that NLS alone did not increase cytotoxicity relative to Accum-modified T-DM1. NLS-modified T-DM1 conjugates had 1.8- to 5.8-fold more potent cytotoxicity values in comparison to unmodified T-DM1. This is consistent with the NLS tagging of the therapeutics approach where there can be an increased cytotoxic effect, and it demonstrates how Accum further enhances cytotoxicity through the added feature of endosome escape.

Accum-modified Tmab also showed no cytotoxicity relative to Tmab against SKBR3 (Figure 3D) and BT474 cells that contain high HER2 expression levels (Figure S2). BT474 cells are insensitive to Tmab, again, due to poor internalization kinetics.[42,56] These data indicate that Accum modification that enables effective nuclear localization for T-DM1 improved the cytotoxic effectiveness by 9- to 18-fold and did not abrogate specificity of T-DM1 for HER2. In addition, these findings support earlier reports that Accum is essential for nuclear localization, and, hence, effective cytotoxicity.

Biochemical Work-Up of Accum-T-DM1 as the Bait for Nuclear Transport Proteomics

As Accum enabled T-DM1 to escape entrapment by as early as 0.5 h from the initiation of incubation with SKBR3 cells, we aimed to quantify the cellular uptake in order to identify a time point that was appropriate to maximize the chances for Accum-NTR interactions in the context when Accum-T-DM1 was abundantly diffused in the cytoplasm after endosome escape. We previously showed that Accum modification of Tmab did not cause cytotoxicity, demonstrating that the molecular processes of escaping endosome entrapment and localizing to the nucleus were benign (Figure 2D; Figure S2). Nonetheless, it was important to check whether the process of endosome escape and diffusion into the cytoplasm, in the context of Accum-modified T-DM1, was not associated with unwanted cytotoxicity within the maximum Accum-NTR interaction time period.

A time course of HER2 binding and cellular uptake revealed that the rate of association for both ADCs increased smoothly and asymptotically toward equilibrium at 2 h (Figure 4A). T-DM1 and Acc$_M$-T-DM1 reached equilibrium at approximately the same rate and indicated that Accum modification did not disrupt the normal HER2 binding and internalization process. The dissociation constant (K_D) values for T-DM1 and Acc$_M$-T-DM1 were 7.0 and 13.5 nmol/L, respectively. SKBR3 cells incubated with T-DM1 and Acc$_M$-T-DM1

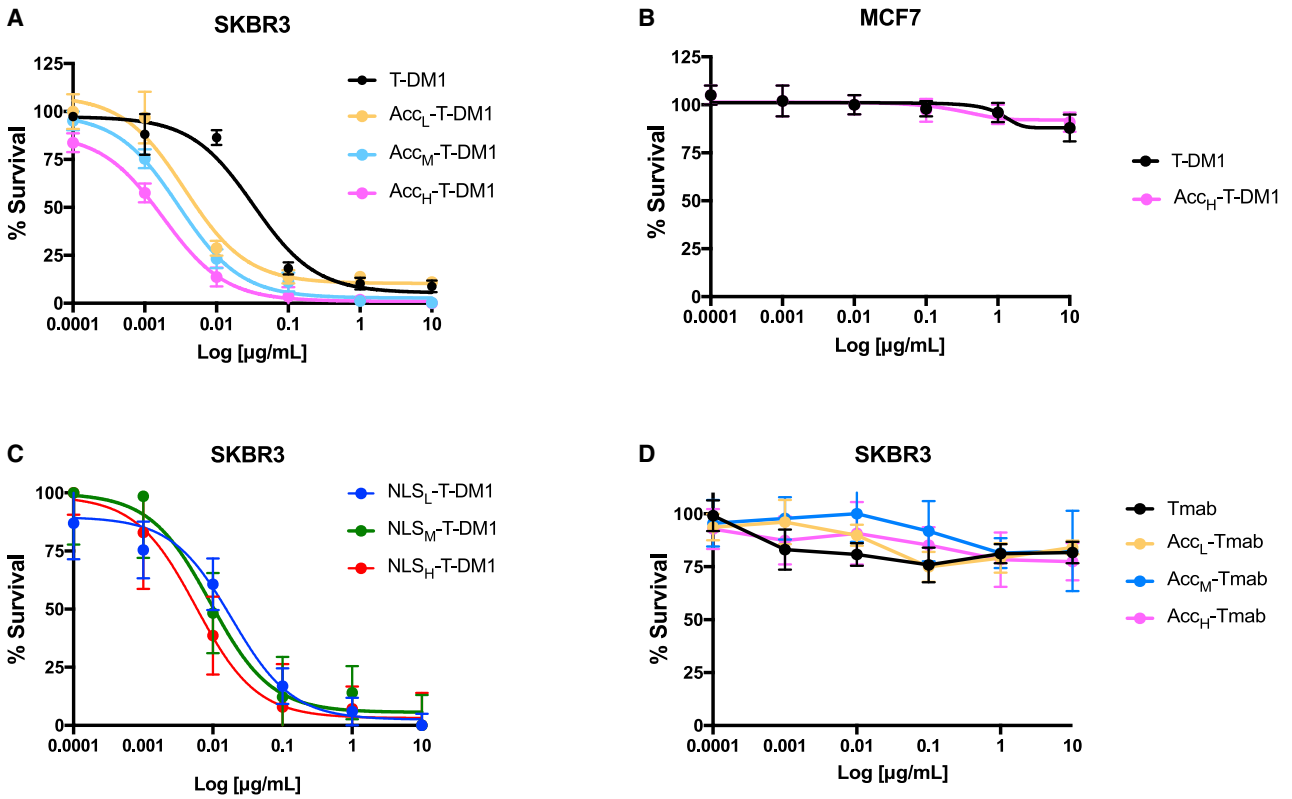

Figure 3. Accum-T-DM1 Cytotoxicity Profile

Dose response relationship on the % survivalof HER2-high SKBR3 treated with (A) Accum-modified T-DM1 conjugates, (C) NLS-modified T-DM1 conjugates and (D) Accum-modified trastuzumab (Tmab) conjugates. (B) HER2-low MCF7 cells incubated with T-DM1 and AccumHigh (Acc_H)-T-DM1. Experiments were performed in triplicate and error bars are shown.

were stained with propidium iodide (PI) to ascertain nucleic acid integrity. With T-DM1 incubation, there was a 15% increase in PI-positive staining at 2 h (Figure 4B). In contrast, there was a <2% increase in PI staining for Acc_M-T-DM1 at 2 h. In combination with the intracellular distribution analyses evaluated by confocal microscopy (Figure 2), these data suggest that the mode of delivering DM1 by Accum-modified T-DM1 is temporally slower than that for T-DM1. In contrast, HER2 rapid recycling in SKBR3 cells results in quicker T-DM1 degradation and payload release relative to Acc_M-T-DM1. Taken together, the cellular uptake combined with the confocal microscopy and PI staining data suggested that 2 h allowed for maximum Accum-NTR interaction between the event of endosome escape and the induction of cytotoxicity and was an appropriate time point to evaluate the use of proteomics. The lack of PI staining at 2 h also suggested that this time point decreased the likelihood of protein expression changes occurring due to cellular stress from the cytotoxic action from DM1.

As Tmab is the predominant component of Accum-T-DM1 based on molecular size, an antibody affinity pull-down with protein G-coated beads was chosen (Figure 4C). ADCs face a particular challenge for this type of pull-down since the conjugated payload may block protein G binding sites. This is further augmented with the addition of various amounts of Accum moieties. Thus, it was important to characterize the pull-downs of lysates from various live SKBR3 cells treated with Accum-T-DM1 conjugates before progressing to the proteomic stage.

A concentration of 7.5 mg/mL (~50 nmol/L) of various Accum-T-DM1 conjugates incubated with increasing amounts (1×10^6 to 15×10^6) of SKBR3 cells was tested at the previously identified 2-h incubation time point. We identified that 15×10^6 SKBR3 cells provided sufficient pulled-down antibody/ADC, as visualized by SDS-PAGE. Figure 4C shows the pull-down efficiency of protein G-coated magnetic beads for the Accum-T-DM1 conjugates relative to Tmab and T-DM1. The amount of Tmab pulled down from treated SKBR3 cells was comparable to a 5-µg standard of Tmab added to protein G-coated magnetic beads. Relative to the artificial Tmab standard, the amount of T-DM1 pulled down was noticeably reduced. The amount of all of the Accum-T-DM1 conjugates pulled down was reduced relative to T-DM1. In fact, in cells treated with Acc_H-T-DM1 there was no visual antibody present on the gel corresponding to the molecular masses of the HC and LC. Only Acc_L-T-DM1 was pulled down at comparable, albeit reduced, levels relative to

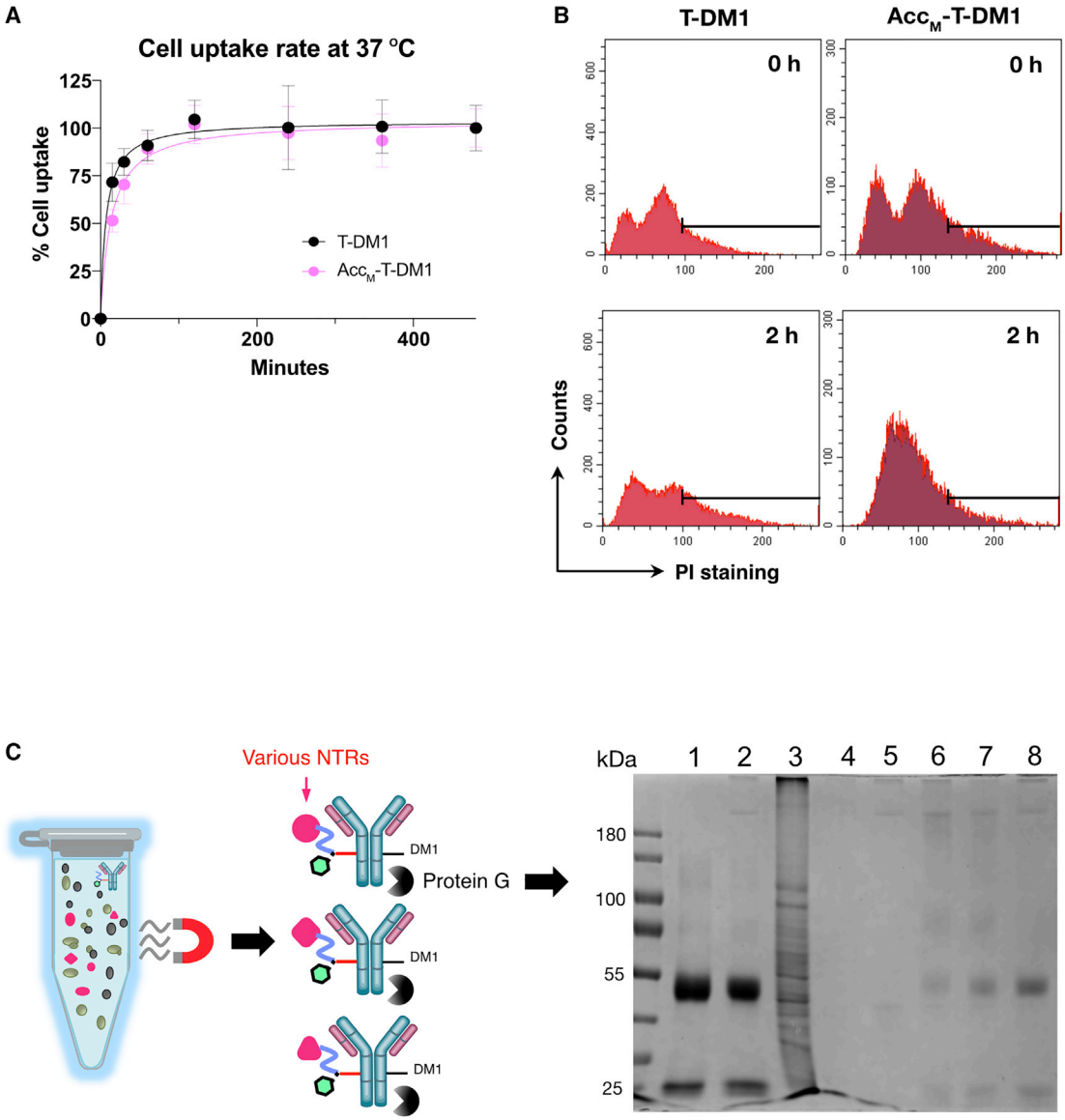

Figure 4. Biochemical Work-Up of Accum-T-DM1 as a Proteomic Bait for Nuclear Localization Analysis

(A) Flow cytometric analysis of % cell uptake time course using 1 μg/mL of T-DM1 and Acc$_M$-T-DM1. (B) Flow cytometric analysis of propidium iodide (PI) staining after conjugate treatment. (C) Schematic of pull-down method depicting Accum-T-DM1 conjugates interacting with various NTRs and pulled down with protein G. Representative Coomassie-stained reduced SDS-PAGE from protein G pull-downs of lysates from SKBR3 cells treated with Tmab, Acc$_H$-T-DM1, Acc$_M$-T-DM1, Acc$_L$-T-DM1, and T-DM1 (lanes 2, 5, 6, 7, and 8, respectively) are shown. Lane 1 is a pull-down of 5 μg of Tmab where there was no treatment of cells. Lane 3 is cell lysate with no pull-down. Lane 4 is the pull-down using beads only. The ladder in kDa is shown on the left. Experiments were performed five separate times.

T-DM1. Based on these results, for its ability to localize to the nucleus, to enhance cytotoxicity, and for its ability to be pulled down by protein G-coated magnetic beads, Acc$_L$-T-DM1 was the agent utilized for proteomic evaluation of nuclear transport.

Bait-Prey Approach for Proteomic Identification of Accum-Specific Interactors

We created a bait-prey method based on two complementary interaction model systems to determine the Accum-specific interactors by significance analysis of interactome (SAINT). The 1,700 unique protein groups identified by mass spectrometry from the co-immunoprecipitated proteins (Table S1) were fed into SAINT. Tmab and T-DM1 were chosen as the references for the differential elimination of nonspecific prey proteins against the antibody backbone and drug DM1, respectively. The first bait-prey approach is herein referred to as the 1 bait:3 control (I:III) model (Figure 5A). Beads-only controls were utilized, as they are a traditional negative reference for pull-down experiments. Because this proteomic analysis of a

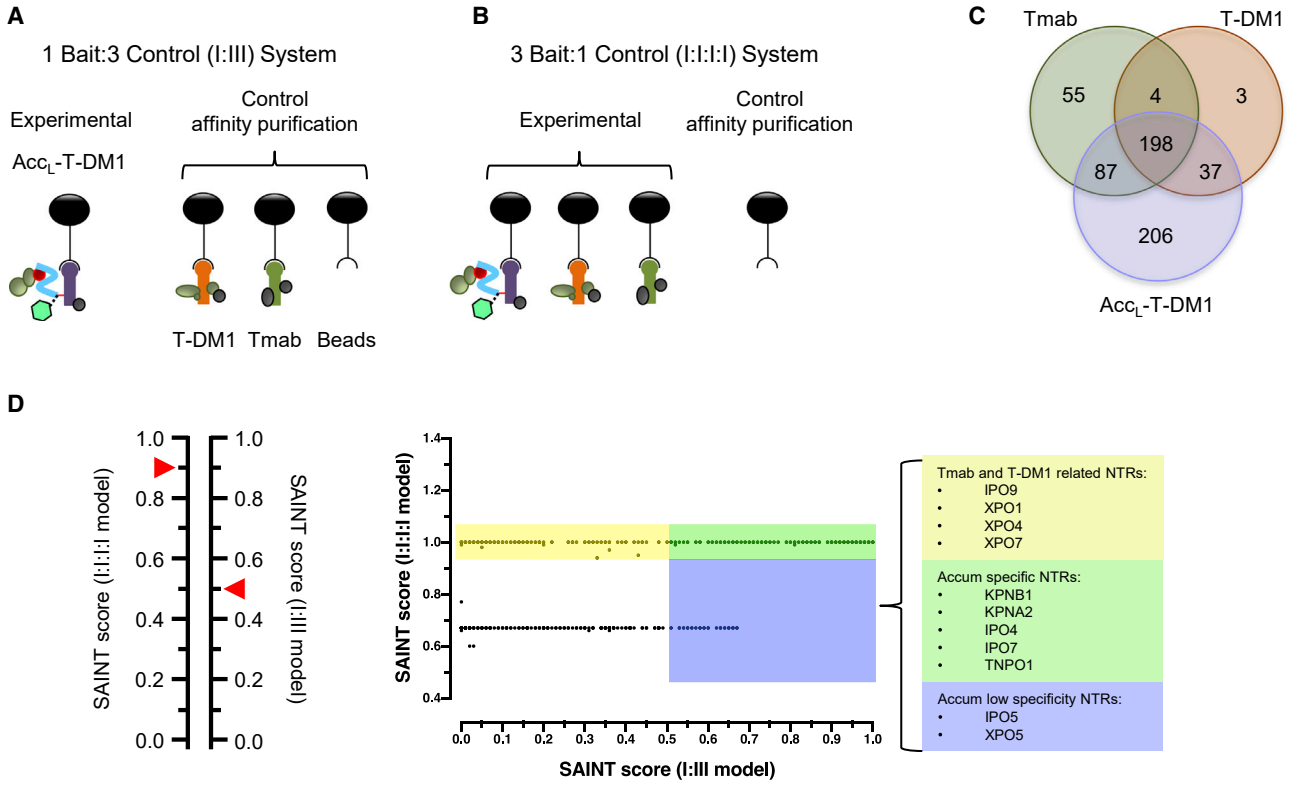

Figure 5. Two-system Proteomic Approach for Evaluating Nuclear Transport

(A and B) Interaction system for (A) Acc$_L$-T-DM1 as a single bait with multiple controls (I:III model) or (B) Acc$_L$-T-DM1, T-DM1, and Tmab as independent baits and a single common control (I:I:I:I model). (C) I:I:I:I Venn diagram of enriched interactors. (D) Left panel: schematic of the two-model system with adjustable SAINT score scales for either the I:III or I:I:I:I models. Red arrowheads indicate the 0.9 and 0.5 thresholds for the I:I:I:I and I:III models, respectively. Right panel: prey enrichment (SAINT score) distribution plotted for Acc$_L$-T-DM1 in the I:III model (x axis) versus the I:I:I:I model (y axis). The blue box covers proteins above the 0.5 threshold (I:III), the yellow box covers protein above the 0.9 threshold (I:I:I:I), and the green box covers proteins that meets both thresholds (>0.5 in I:III and >0.9 in I:I:I:I). These results come from pooled data from four independent biological replicates.

NLS-modified agent for evaluating nuclear transport had never been performed, we identified interactors based on a primary (high-confidence) and a secondary (medium-confidence) SAINT score (STSc) thresholds that were set at $\geq$0.9 and $\geq$0.5, respectively. The statistics are summarized in Table S2. Using the cutoff threshold STSc $\geq$0.9, only a single NTR, KPNB1, was present among 106 interactors. This was uncharacteristic since importin-β requires importin-α to form the classical nuclear transport complex for types of NLS sequences contained in Accum. This suggested that the I:III system used in combination with an STSc $\geq$0.9 was overly stringent to identify potential NTR interactors. In contrast, using the cutoff of STSc $\geq$0.5 that now contained 275 interactors, in addition to importin-β, we identified the NTRs IPO7, importin-4 (IPO4), importin-5 (IPO5), transportin-1 (TNPO1), and importin-α1 (KPNA2).

For the second model, we performed SAINT analyses with Acc$_L$-T-DM1, T-DM1, and Tmab as individual baits and using beads only as the single control, herein referred to as the I:I:I:I model (Figure 5B). The differentiating aspect of the second model was that interactors could be identified that were common and unique between the three baits. As the I:I:I:I model had reduced stringency based on controls, we considered only interactions with STSc $\geq$0.9. The I:I:I:I system identified 528, 242, and 347 proteins identified as interactors for Acc$_L$-T-DM1, T-DM1, and Tmab, respectively (Figure 5C; Table S3). Tmab and T-DM1 had 55 and 3 unique interactors, respectively. In contrast, Acc$_L$-T-DM1 had 206 unique interactors. There were 198 proteins common for all of the baits. The large overlap was most likely due to the mAb Tmab, the only common feature shared by all three baits. Using the I:I:I:I model, there was an abundance of proteins with 10- to 300-fold enrichment for Acc$_L$-T-DM1 relative to T-DM1 and Tmab (Figures S3A and S3B). Importantly, by combining the I:I:I:I and I:III models with the STSc $\geq$0.9 and $\geq$0.5 cutoffs, respectively, we were able to identify NTRs that were specifically and significantly enriched for Acc$_L$-T-DM1 (Figure 5D). Thus, both models provided results in agreement with each other, and together they strengthen the certainty that the identified NTRs were Accum-specific interactors.

With this prey-bait proteomic method it was also possible to characterize the expanding intracellular interaction network for Acc$_L$-T-DM1. Because Accum has a stretch of positively-charged amino acids,

we evaluated important quality control proteomic characterizations as performed by Lang et al.[57] For example, as polylysine-tagged proteins can present an experimental challenge for controlling nonspecific electrostatic interactions, the molecular weight of interactors can be plotted and analyzed. We found that most Accum-specific interactors had molecular weights of 10–30 kDa, and there was a depletion of larger proteins (Figure S4A). Proteins between 10 and 30 kDa accounted for 50% of the Accum-specific interactors. A boxplot analysis demonstrated that there was a significant difference between distributions of molecular weight of Accum interactors and of all identified proteins (Figure S4B). Similar to the findings by Lang et al.,[57] enrichment of low-molecular-weight proteins indicates specific interactions and further supports that the identified interactome is Accum-specific. Thus, we created a two-model system calibrated for two different STScs that when analyzed together were essential to support Accum-specific interaction confidence.

Molecular Topology of Protein Interaction Modules for Acc_L-T-DM1

The enriched interactors specific for Accum-T-DM1 from the SAINT analysis (I:III model) were entered into GeneMANIA (GM) in Cytoscape to determine enriched biological processes (Tables S2 and S4). Gene set enrichment analysis (GSEA) was performed by GM to highlight the most enriched Gene Ontology (GO) terms and used to systematically attribute a "generic pathway" to each protein in the network according to their main function.[58,59] We identified 164 GO terms or pathways that were significantly enriched for Acc_L-T-DM1 (Table S4). We identified 15 protein families or common cellular pathways that were significantly enriched in the dataset (Table S2). Cytoscape allowed us to obtain an aerial overview of the interaction network by clustering proteins based on these protein families/pathways (Figure 6A). The top five most enriched protein families/pathways were exclusively composed of ribosomes involved with unique cellular functions, including nuclear transport (Figure 6B; Table S4).

For the I:I:I:I model, genes obtained from the SAINT analysis with an STSc $\geq$0.9 were entered into GM (Tables S3 and S5). There were 310 GO terms identified for Acc_L-T-DM1, 231 for T-DM1, and 271 for Tmab. Of these, 192 were common between all three baits, and 73 were unique to Acc_L-T-DM1 (Figure S5A). The top five pathways represented in Figure 6 were also strongly enriched using the I:I:I:I model (Figure S5B). Importantly, only Acc_L-T-DM1 had the "protein import into nucleus" GO term enriched. Thus, the I:III and I:I:I:I models generated overlapping data, further confirming that this analytic proteomic method was specific for Accum. Also noteworthy, heat shock proteins that are the main mediators of cellular stress response were not enriched or specific for Accum in either the I:I:I:I or I:III model. This supports our cytotoxicity and flow cytometric studies in Figures 3D and 4B, respectively, that Accum-enabled endosome escape is not cytotoxic but rather a benign escape mechanism to access the cytosol.

NTR Interactors

The affinity purification after cell treatment revealed unanticipated findings for NTRs interacting with Acc_L-T-DM1. As anticipated, the classical NTRs importin-α and importin-β strongly interacted with Accum (Figure 7A). However, the non-classical NTRs IPO4, IPO5, IPO7, and transportin-1 also interacted strongly with Accum. In fact, the non-classical NTR IPO7 was the most abundant off all NTRs with an average spectral count (AvgSpec) of 28.67 (STSc = 0.66). NTRs below the 0.5 STSc threshold included importin-β3, importin-8 (IPO8), importin-9 (IPO9), importin-11 (IPO11), and karyopherin subunit α4 (KPNA4). The STScs, average spectral count, and Bayesian false discovery rate (BFDR) are found in Table S3 and summarized in Table S6.

Figure 7B shows the dot plot generated from the I:I:I:I model to further demonstrate the specificity of enriched NTRs for Accum. The dot plot shows that IPO7 had a strong increase in relative abundance and average spectral count for Acc_L-T-DM1 relative to T-DM1 and Tmab. All NTRs with the exception of IPO9 with an STSc 0.9 from Figure 7A were enriched in SKBR3 cells treated with Acc_L-T-DM1 relative to Tmab and T-DM1. As the STSc was $\geq$0.9 for all three baits in the dot plot, the abundance of the NTR enriched is the defining factor and IPO7 is the most abundant.

Western blot was used to biochemically confirm the relative abundance of protein in the pull-down assays from lysed SKBR3 cells previously treated with Acc_L-T-DM1, T-DM1, or Tmab. Among the importins evaluated, IPO7 was the most abundantly present NTR (Figure 7C). More importantly, the presence of IPO7 was only present with pull-downs for Acc_L-T-DM1 relative to T-DM1 or Tmab. As anticipated, IPO7 was not present in the beads-only control. For the classical NTRs, the presence of importin-β was increased relative to importin-α, which also confirmed the proteomic data. Importin-α and importin-β were also present in the T-DM1 and Tmab pull-downs, albeit at reduced amounts compared to Acc_L-T-DM1. IPO4 appeared to be only slightly less abundant in the T-DM1 and Tmab pull-downs compared to Acc_L-T-DM1. This matched well with the dot plot, as IPO4 had only a slightly increased average spectral count compared to Tmab. Thus, this biochemical analysis of NTR protein in the pull-down assays validated the findings from the proteomic data obtained from the I:I:I:I model.

Acc_L-T-DM1 Cytotoxic Effectiveness Is Reliant on IPO7-Mediated Nuclear Transport in SKBR3 Cells

The ability to use RNA interference as a tool for gene silencing was utilized to determine whether an NTR identified in this proteomic method was essential for Accum's ability to enhance T-DM1 cytotoxic potency. SKBR3 cells were transfected with small interfering RNA (siRNA) pools individually targeting KPNA2, KPNB1, IPO4, IPO7, and siRNA control followed by lysing cells at 24 and 96 h post-transfection. Expression of indicated gene products targeted for silencing was evaluated at 24 and 96 h post-transfection to coincide with the initiation and termination of the 72-h cytotoxicity assays of SKBR3 cells with T-DM1 and Acc_L-T-DM1. Western blots confirmed the reduction in protein levels for all four NTRs at 96 h (Figure 8A) but not at 24 h (Figure S6A) post-transfection. There was a <2-fold reduction of the tested importins at 24 h (Figure S6B).

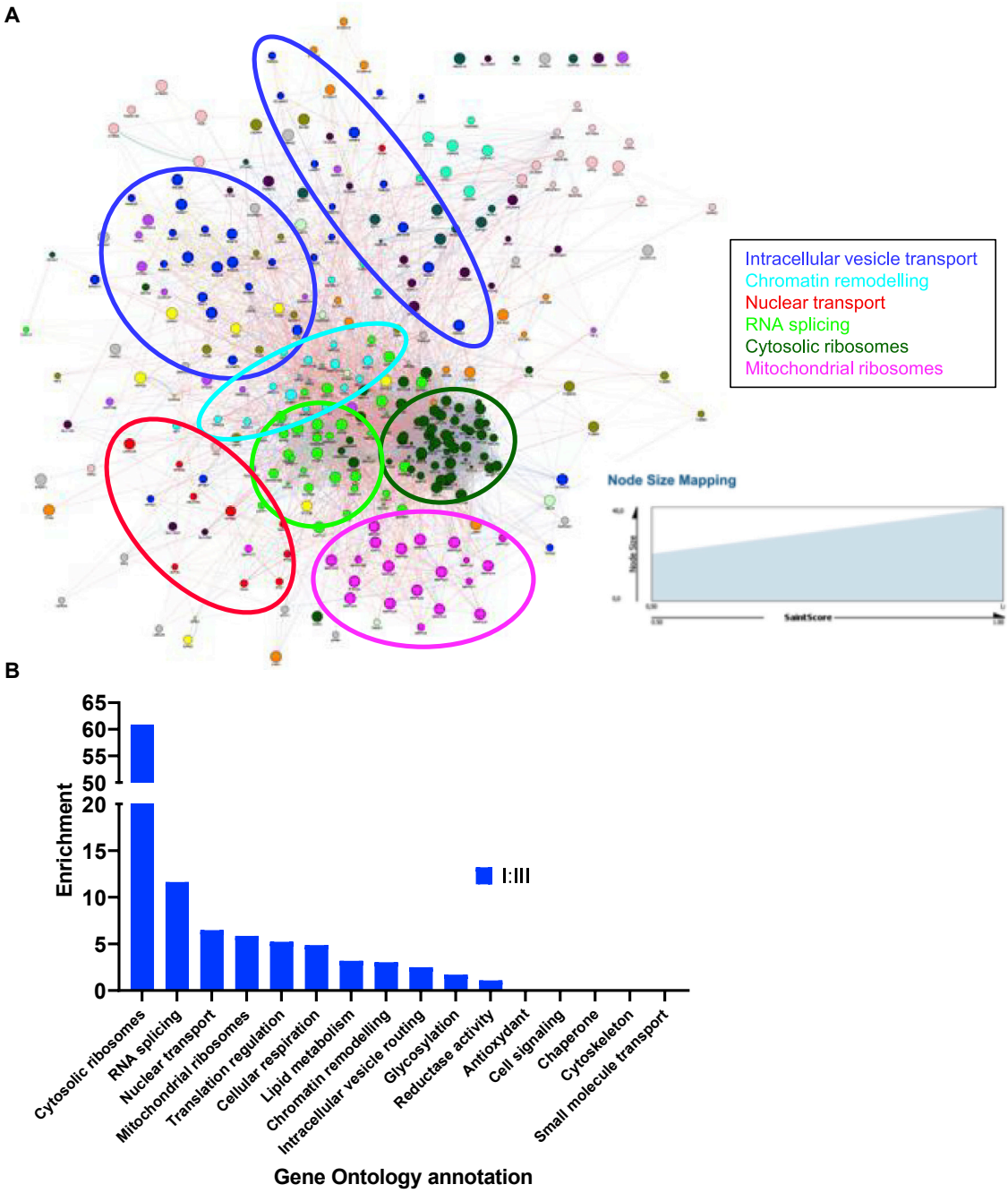

Figure 6. Accum-specific Interaction Network

(A) Aerial view of GeneMania network of generic pathways or protein families that interact with Acc_L-T-DM1 in the I:III system generated in Cytoscape. Node size is proportional to the SAINT score (see the node size mapping box). (B) Ranking of Accum-specific interactors based on enrichment of GO values. Enrichment scale is $\log_{10}(1/q \text{ value})$.

At 96 h, the reduction in expression was >2-fold for IPO7 and IPO4. Reductions for KPNA2 and KPNB1 remained <2-fold at 96 h. Transfections with scrambled pools did not cause a reduction in NTR protein expression (Figure 8A).

Acc_L-T-DM1 cytotoxicity was dependent on non-classical IPO7-mediated nuclear transport. The IC_{50} values for Acc_L-T-DM1 were very similar (range, 0.0040–0.0044 μg/mL) on SKBR3 cells transfected with siRNA pools to knock down KPNA2, KPNB1, and

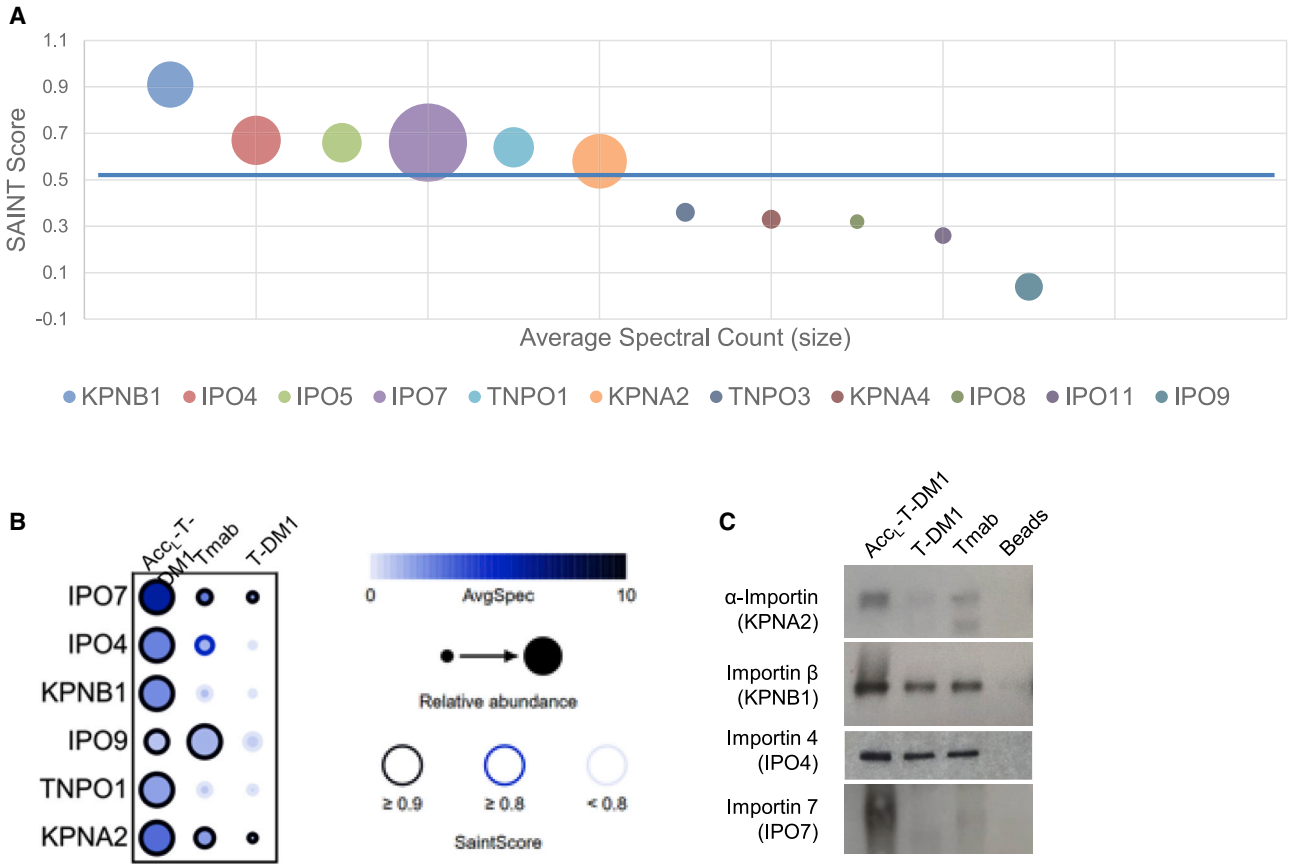

Figure 7. Accum-specific Imortin Interactors

(A) Bubble plot showing the SAINT score enrichment and overall abundance (dot size) of the identified NTRs. The cutoff is indicated by the blue line. (B) Dot plot output showing quantitative SAINT interactions between Acc$_L$-T-DM1, Tmab, and T-DM1 and the NTRs found in the I:I:I:I system. The confidence of the detected interaction is shown as the circle edge, with black being high confidence (StSc ≥ 0.9), blue being medium confidence (StSc ≥ 0.8), and light gray being low confidence (StSc < 0.8). Circle size indicates the prey's relative abundance across baits. The bait that yielded the highest spectral count for a prey is given as a full-sized circle, and the circle sizes for the other baits are scaled relative to this maximum. The color scale bar of the circles indicates the prey's spectral count for the corresponding bait. (C) Confirmation of the NTR-Accum interaction by affinity purification followed by a western blot against the indicated preys. Experiments were performed in triplicate.

IPO4 relative to non-transfected SKBR3 cells and cells transfected with scrambled siRNA pools (Table S7; Figure 8B). However, Acc$_L$-T-DM1 had a 3-fold loss in cytotoxic potency in SKBR3 cells when IPO7 was knocked down. When the same transfected SKBR3 cells were treated with T-DM1, the IC$_{50}$ values were all comparable to each other (Table S7; Figure S7). Importantly, the cytotoxicity potencies for Acc$_L$-T-DM1 and T-DM1 for non-transfected SKBR3 cells were consistent with IC$_{50}$ values from the previously treated SKBR3 cells, as shown in Figure 3A.

Surprisingly, knockdown of the classical NTRs importin-α and importin-β did not affect Acc$_L$-T-DM1 cytotoxicity potency. SKBR3 cells with KPNB1 knockdown had increased survival by approximately 20% when challenged by both Acc$_L$-T-DM1 and T-DM1 at concentrations of 0.1–10 μg/mL (Figure 8B; Figure S7). We observed that KPNB1 knockdown of more than 2-fold was lethal to cells. This is consistent with the known observation that breast cancer cells, including SKBR3, have a reliance on KPNB1 for growth and survival.[60] Thus, the increased presence of KPNB1, due to the inability to not increase knockdown without unwanted cell death, is a plausible explanation for why the cells are difficult to kill even at the higher concentrations of Acc$_L$-T-DM1 and T-DM1 (Figure 8B; Figure S7). Nonetheless, the IC$_{50}$ values for KPNB1 knockdown were very similar to the IC$_{50}$ values in SKBR3 cells with KPNA2 and IPO4 knocked down (Table S7). More importantly, the cytotoxic potency of T-DM1 in SKBR3 cells transfected with siRNA pools to knock down IPO7 was unchanged relative to non-transfected cells and the knockdown of KPNA1, KPNB1, and IPO4.

To visually confirm that IPO7 indeed mediated nuclear localization of Acc$_L$-T-DM1 and, hence, is the NTR responsible for its enhanced cytotoxicity, we performed confocal microscopy in IPO7 knocked down SKBR3 cells. We observed a strong fluorescent punctate pattern in the nucleus of SKBR3 cells transfected with siRNA control pools

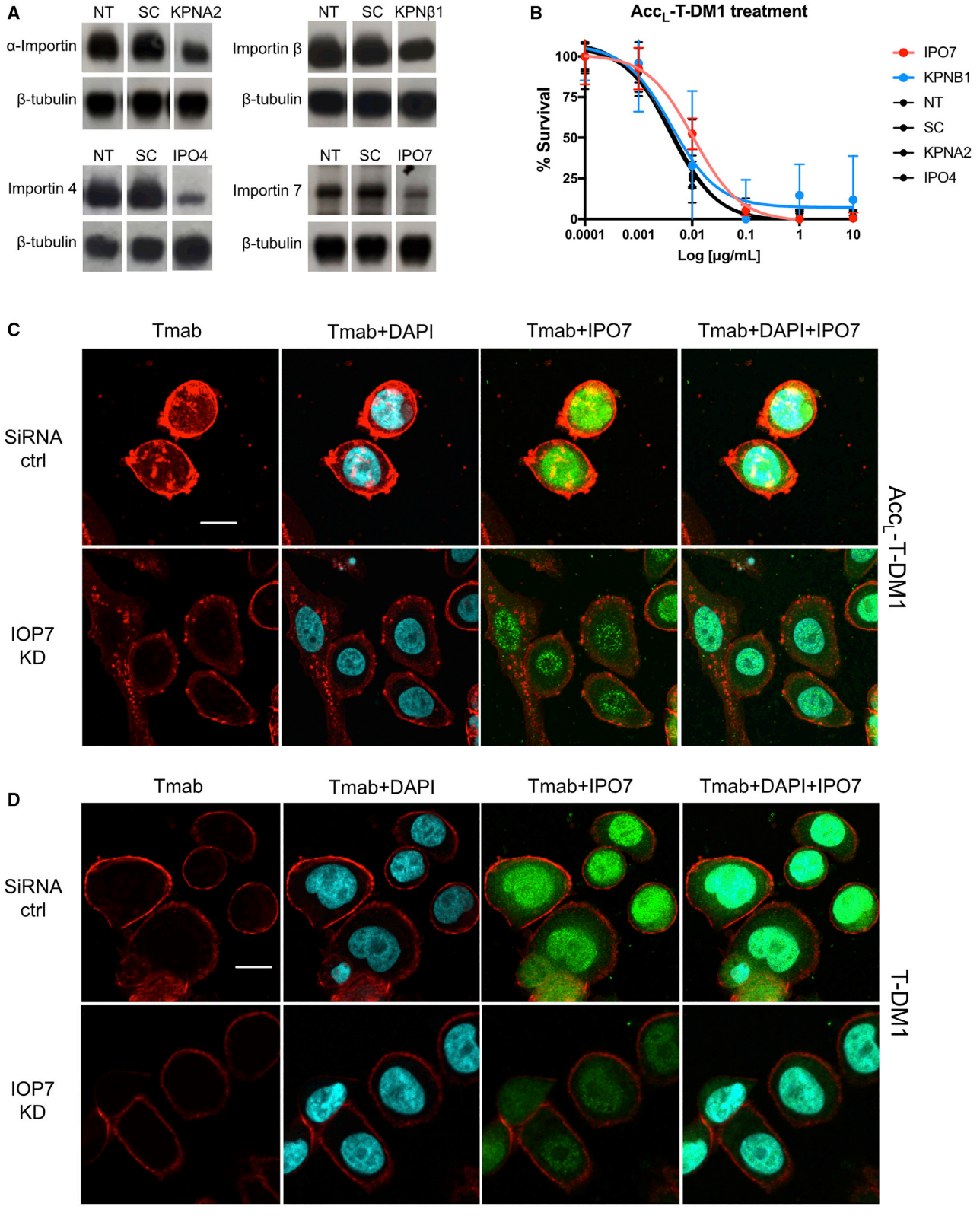

(legend on next page)

that was specific for Acc_L-T-DM1 (Figure 8C). We observed the same highly linear mode of Acc_L-T-DM1 being delivered to the nucleus starting at endosome escape, nuclear transport, and finishing with release and accumulation inside the nucleus, as shown in Figure 2. There was a strong signal also present, indicating an abundance of IPO7 in the nucleus and cytoplasm. In contrast, SKBR3 cells transfected with siRNA pools that knock down IPO7 showed no nuclear localization of T-DM1 (Figure 8D). This was most likely due to the suppression of IPO7 expression, as there is notably less fluorescent signal in knocked down to non-knocked down SKBR3 cells (Figure 8C and 8D). In SKBR3 cells transfected with siRNA control or IPO7-specific pools and treated with T-DM1, there is no nuclear localization. This demonstrated that Acc_L-T-DM1 nuclear transport specifically relied on IPO7 and further suggested that IPO7 was the key NTR regulator for Accum-mediated shuttling of T-DM1 to the nucleus for enhancing cytotoxicity in SKBR3 cells.

Analysis of IPO7 Binding to H1.0 implies That Electrostatic Interactions Drive Acc_L-T-DM1 Recognition

Structural analyses have been instrumental for explaining how the cNLS is recognized by importin-α. Importin-α has a curved solenoid structure composed of 10 armadillo (ARM) repeats.[61] Hydrophobic, electrostatic, and polar interactions contribute to the ability of importin-α to recognize cNLS. It has previously been shown these binding forces encompass a 1,314-$Å^2$ surface area with 149 contacts <4 Å buried between the cNLS and importin-α in the major binding site.[62] The minor binding site has a contact surface area of 1,194 $Å^2$ with 110 contacts of <4 Å. The cNLS sequences bind in an extended conformation with the peptide running antiparallel to the directions of the ARM repeat helices (Figure S8A). The base of the cNLS-binding pocket contains the major interactions dominated by the H3 helices. Residues that are highly conserved in these pockets are tryptophans, asparagines, and tyrosines (Figure S8B). Interestingly, acidic residues that are in sufficient proximity to form electrostatic bonds are at the periphery of the deepest point in the binding pocket (Figure S8B). These acidic residues play only supporting roles for overall cNLS binding strength. Alternatively, the conserved tryptophan and asparagine form a three-dimensional topography for cNLS to position itself on based on several polar hydrogen bonding and hydrophobic interactions. Because cNLS binding is generally accepted to bind importin-α in this fashion, it was perplexing why Accum that harbors a cNLS from SV40 large T antigen was not preferentially recognized by importin-α.

In contrast to ARM repeats, IPO7, as well as the importin-β family, is composed almost entirely of HEAT repeats. Although ARM and HEAT repeats stem from a common phylogenetic origin, HEAT repeats are much more variable in length, amino acid sequence, and three-dimensional structure.[61,63,64] Recently, Ivic et al.[65] determined the cryo-EM structure of human IPO7 in complex with importin-β and histone 1 (H1.0). Their study revealed numerous acidic residues lining the inner concave surface and a unique ~90-aa-long acidic-rich loop at the C terminus that most likely drive binding and transport of Acc_L-T-DM1 (Figure 9A). Rather than a conserved array of tryptophans, asparagines, and tyrosines that drive cNLS binding, the authors discovered that IPO7 forms a heterodimer with importin-β that forms a cradle for the positive supercharged protein H1.0. Based on the results in the present study and from the elucidations from Ivic et al.[65] on IPO7 binding of H1.0, it is highly probable that IPO7 binds Accum based on electrostatic interactions. A potential model is that the positive-charged Accum, similar to the C-terminal tail of H1.0, is cradled in a negative-charged cage formed from the acidic amino acids lining the inner concave surface of the HEAT repeats and the super-acidic C-terminal loop that acts as a flap on the opposing side of the NLS (Figure 9B).

DISCUSSION

We developed an approach designed to create a novel biopharmaceutical that could overcome the current limitations to the trade-off concerning increased cellular accumulation versus target cell specificity and in parallel provide a generally applicable methodology for elucidating dominant nuclear transport pathways for NLS-tagged therapeutics. The surprising results have also opened interesting questions for researchers developing tools to study nuclear transport or for the development of NLS-based biopharmaceutical agents. Although evidence of nuclear transport is showing that NTRs can be selective for endogenous cellular cargos depending on cell type or cellular states, NLS-modified agents continue to operate on a "hit-and-miss" approach, particularly for therapeutic development. Thus, approaches that can provide rational therapeutic design of NLS-based agents and also acquire cellular insights due to nuclear transport could potentially impact the fields of intracellular targeting of therapeutic agents and fundamental NTR biology.

In this study, the Accum platform demonstrated that when conjugated to the clinically approved anti-HER2, biopharmaceutical T-DM1 (Figure 1B) was able to localize to the nucleus of SKBR3 cells and increase cytotoxicity by up to 18-fold (Figures 2 and 3A). In addition, a cellular treatment coupled to affinity pull-down (Figure 4C) and the proteomic method (Figures 5A, 5B, and 5D) was developed that is theoretically applicable for any NLS-modified therapeutic agent. In the SKBR3 model of HER2-positive breast cancer, the developed proteomic method allowed us to discover that the strongest NTR-specific interactor for Accum-T-DM1 was IPO7 (Figures 7A–7C). The dependency of Accum-T-DM1 on IPO7 for its ability to

Figure 8. Accum-T-DM1 Nuclear Localization Is Dependent on Importin-7

(A) Silencing of KPNA2, KPNB1, IPO4, and IPO7 genes at 96 h post-transfection and the western blot images of the corresponding proteins importin-α, importin-β, importin-4, and importin-7. β-Tubulin was used for the loading control. NT, not transfected; SC, scrambled siRNA. (B) % Survival curves and error bars for Acc_L-T-DM1 after 72 h of treatment of SKBR3 cells NT and transfected with siRNA pools specific for indicated NTR genes or scrambled (SC) sequence. (C and D) Representative confocal microscopy images of SKBR3 cells transfected with siRNA control or IPO7-specific pools and then incubated with (C) Acc_L-T-DM1 or (D) T-DM1. Cells were stained for Tmab (red), nucleus (cyan) and importin-7 (green). Knock-downs, cytotoxicity assays, and confocal microscopy experiments were all performed in triplicate. Scale bars, 100 nm.

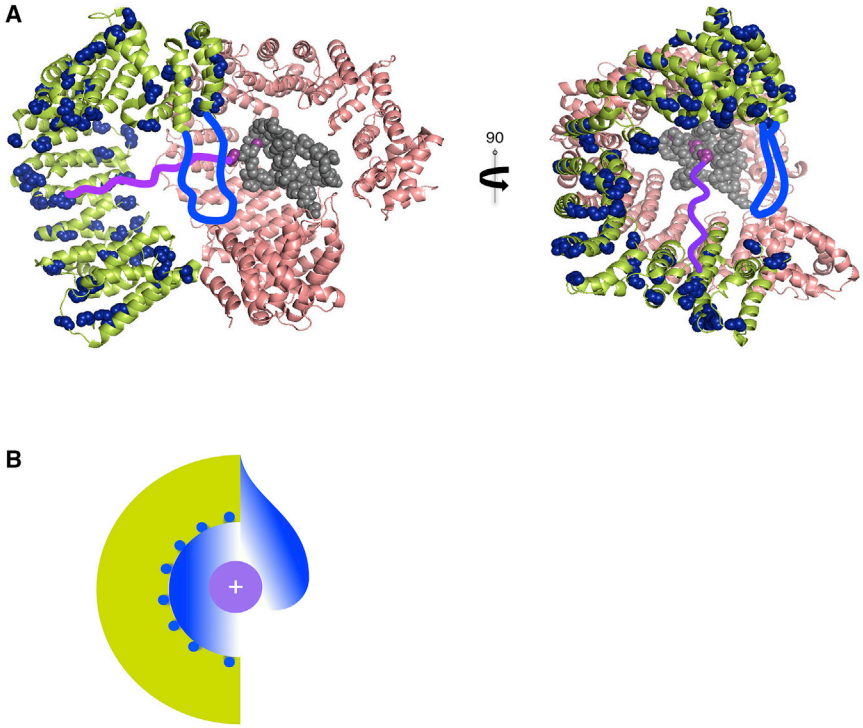

Figure 9. Importin-7 Binding to Accum is Reliant on Charge

(A) Images from PDB: 6N88 showing importin-7 (lime-colored ribbons) decorated with acidic residues (blue spheres) in complex with importin-β (salmon-colored ribbons) and H1.0 (gray spheres). The acidic loop (blue) of importin-7 and C-terminal-positive supercharged tail purple spheres that represent the stem of the tail are shown. The purple sinuous line is not in PDB: 6N88 and is schematically presented. (B) Proposed model of importin-7 recognition of the cNLS harbored by Accum. The inner positive-charged NLS (purple) is bound by an electrostatic cradle composed of a negatively charged environment (blue color) composed of the deep pocket in the HEAT repeats and a negatively charged flap from the acidic loop.

improve tumor killing was demonstrated when its gene IPO7 was knocked down (Figure 8A) followed by treatment with Acc_L-T-DM1 (Figure 8B) and T-DM1 (Figure S7). The IC_{50} value in IPO7-knocked down cells treated with T-DM1 remained unchanged relative to non-knocked down cells. In contrast, the IC_{50} value for Acc_L-T-DM1 was decreased by 3-fold relative to the value obtained from the non-knocked down SKBR3 cytotoxicity assay. Confocal microscopy visually confirmed that when IPO7 was knocked down, Acc_L-T-DM1 nuclear localization was abrogated (Figure 8C). Importantly, this suggested that the classical NTR complex of importin-α and importin-β was not required for nuclear transport and, hence, was the reason why knockdown of the genes KPNA2 and KPNB1 did not affect cytotoxicity of Acc_L-T-DM1.

Approximately one decade ago, Rix and Superti-Furga[66] addressed the need of the pharmaceutical community to utilize proteomic profiling to better understand the interactions within cells of small molecules, which has led to strong activity in this research domain. In contrast, studies on proteomic profiling of biopharmaceuticals with respect to their dynamics inside cells are scarce. Only recently has there been important advances that have utilized proteomic profiling to determine resistance mechanisms to biopharmaceuticals such as Tmab, T-DM1, and other emerging mAb-based drugs.[41,67–69] However, these approaches have not specifically addressed intracellular transport. Mechanistic insights into intracellular transport of macromolecular therapeutics using proteomic approaches have only been reported for nanoengineered particles.[70,71] These studies were essential, as they elucidated key intracellular transport regulators and, hence, have advanced the development of these particles.[72] Therefore, this approach could also be adapted to provide novel insights on nuclear transport pathways and improved effectiveness for NLS-modified therapeutic agents.

It was important to develop a method whereby Accum-T-DM1, T-DM1, and Tmab were allowed to mix with live cells. The major challenge is to have a sufficient amount of antibody for subsequent pull-downs without killing the cells. An added challenge was that pull-down efficiency was reduced due to Accum tagging to T-DM1 (Figure 4C). Thus, we evaluated treatment in cell numbers ranging from 1×10^6 to 15×10^6 per incubation. In this study, our main goal was to incubate cells with a sufficient amount of ADC that would not cause cytotoxicity. A time point of 2 h was selected based on maximum cell uptake without causing cell death (Figures 4A and 4B). Endo et al.[73] used T-DM1 as bait to determine that DM1 binds a cell surface protein cytoskeleton-associated protein 5 (CKAP5) that is expressed on hepatocytes in the absence of HER2. A concentration of 250 μg/mL (~1,667 nmol/L) T-DM1 was incubated with 1.5×10^6 cells. The study determined that DM1 interaction with CKAP5 is most likely a contributing factor for dose-limiting hepatotoxicity in patients treated with T-DM1. However, the amount of T-DM1 used was well above the IC_{50} value. A direct comparison of cytotoxic potency between CKAP5- and HER2-positive-only cells and T-DM1 was not reported. However, the potent cytotoxic concentration shown for T-DM1 in CKAP-positive/HER2-negative cells ranged from 30- to 142-fold higher than reported IC_{50} values for T-DM1 against HER2-positive cells,[52,53] including in the present study. The method in our study utilized 7.5 μg/mL (~50 nmol/L), which was also well above the cytotoxic IC_{50} values for both Acc_L-T-DM1 and T-DM1. Theses comparative findings indicate the importance of performing additional experiments to evaluate cytotoxicity. This is required if the intent is to analyze live cells that have yet to change gene expression levels due to cytotoxic stress. Nonetheless, this study demonstrates that the amount of ADC utilized is comparable to that found in the study by Endo

et al.,[73] and could potentially be refined for future NLS-tagged therapeutics.

The development of controls was also a significant feature in the proteomic setup. When performing antibody pull-downs, an isotype non-specific IgG would always be used. In this case, an Accum-tagged IgG could be used to confirm Accum-specific interactors without Tmab being present. However, a key aspect in this study, as well as in any future studies, is receptor binding followed by internalization, endosome escape, and nuclear localization in live cells. An Accum-IgG agent would not bind HER2 and internalize and, hence, could not be pulled down by protein G to be analyzed by mass spectrometry. This would prevent any study of nuclear transport, specifically from the time of endosome escape and nuclear localization. Therefore, we developed a dual bait-prey analysis system in combination with controls Tmab and T-DM1 that would bind HER2 and internalize. As Tmab and T-DM1 pull-downs were both analyzed as controls (I:III model) and independent baits (I:I:I:I model), we were able to critically evaluate their interaction overlap to the Accum-T-DM1 interactome. This two-pronged approach included precisely scaled SAINT scoring for each model system and allowed increased discernment of Accum-specific interactors. This tandem analysis resulted in the discovery of IPO7 as the driver of Accum-enhanced T-DM1 cytotoxicity. In addition, careful consideration should be taken for the peptide modification load. The number of peptide moieties for maximizing therapeutic application may not be the load needed for conducting proteomic studies. In this study, we achieved the highest cytotoxicity with Acc_H-T-DM1. However, Acc_L-T-DM1 was the only construct with acceptable protein G pull-down efficiency for proteomic analysis. Thus, the amount of NLS peptide modification needed for proteomic evaluation may not be the same used for treatment.

Although the term "nuclear transport" can have different meanings between scientists studying basic mechanisms and those interested in therapy, the development of SV40 cNLS-modified agents is an area of research that is being actively investigated.[29–34] However, the general consensus is that the mechanism for these NLS-containing drugs is dependent on the importin-α/importin-β complex to achieve nuclear localization.[32–34,74] Our results clearly indicate that the SV40 cNLS as part of Accum is dependent on non-classical nuclear transport, specifically IPO7. However, the development of SV40 NLS-tagged agents for various therapeutic agents is ongoing.[74–79] In addition, different NLS sequence-tagged therapeutics have made significant advances. For example, HIV-1 *trans*-activating protein harbors an NLS and has been extensively utilized for the nuclear delivery of various agents,[80–82] with a few reaching the clinic (ClinicalTrials.gov: NCT01975116 and NCT00914914). However, they have been shown to suffer from target antigen specificity problems.[13,14]

The additional interactors uncovered by the proteomic portion of this study will impact future directions on studying nuclear transport using NLS-modified agents. Most of the human non-classical NTRs are able to recognize unique sets of proteins or RNA, thus creating multiple transport pathways across the nuclear pore complex.[35] IPO7 is known to mediate nuclear transport by forming a heterodimer with importin-β. Recently, Ivic et al.[65] reported on the structure of an IPO7/importin-β/H1.0 complex. This study clearly demonstrated that IPO7 relies on an electrostatic binding mechanism for recognizing H1.0. This supports why the strong interaction of importin-β with Acc_L-T-DM1 was continuously present in the different proteomic analyses used in this study. IPO7 has regions at the extreme N and C termini that interact with importin-β and are required for nuclear localization of H1.0. Based on this study, it appears that IPO7 is only required for recognition and nuclear transport of Accum-T-DM1. Based on the results from this study and from Ivic et al.,[65] a current model for Accum nuclear transport is on its NLS being complexed by a negative charged cradle formed by the acidic residues on the inner concave surface and the negative supercharged loop (Figure 9B). However, we cannot rule out that an IPO7/importin-β complex does exist in SKBR3 cells. IPO7 is also known to be critical for the nuclear transport of ribosomal proteins and histones.[35] Preference for IPO7 versus an IPO7/importin-β heterodimer has been observed for particular nuclear-localized proteins such as EZI and ERK-2 kinase.[83,84] IPO7 has also been shown to transport RBL4 and RBL6 into the nucleus,[85] which were both identified to interact with Acc_L-T-DM1. Thus, this report strongly suggests that transport of Acc_L-T-DM1 is only dependent on single-bound IPO7.

This study suggests that in the context of NLS-tagged therapeutics, charge recognition may dominate the pathways used for nuclear transport and, hence, the efficiency of nuclear localization. Long loops with a high content of acidic residues are also found in IPO4, IPO9, and transportin-1.[65] Transportin-1 and IPO4, but not IPO8 and IPO9, had strong SAINT interaction scores for Accum (Figure 7A). IPO4 that contained the second highest STSc among NTRs was not essential for Acc_L-T-DM1 cytotoxicity. IPO4 is known to bind to only a few known proteins.[35] Interestingly, among them the protein TP2 contains an NLS sequence of GKVSKRKAV. Since this sequence is similar to the NLS sequence contained in Accum, it is logical to conclude that IPO4 also interacted with Acc_L-T-DM1. However, it was not essential for cytotoxicity. Accum was not tested for its reliance on nuclear transport or cytotoxicity with transportin-1. Therefore, it is likely that electrostatic interactions are not the only feature governing Accum binding. Most likely, three-dimensional features that are unique to the NLS therapeutic agent also have an influence on recognition by individual importins. As a consequence, this finding underscores the need to carefully identify the nuclear transport pathway for investigational NLS-tagged therapeutics.

This proteomic and biochemical approach can most likely be adopted for any NLS-modified mAb agent as a foresight for a rational approach for studying nuclear transport mechanics or for the development of therapeutic agents. Thus, this proteomic-based method can be feasibly integrated into development workflows for next-generation NLS-based agents to identify the most dominant NTR pathways in cells of interest. For next-generation NLS-modified biopharmaceuticals, it is profoundly important to understand the tumor

system to optimize the NLS-based approach. Such understandings could be useful in combination with DNA/RNA gene therapy approaches where the NTRs specific for ribosome nuclear transport could synergize to increase nuclear delivery efficiency. For fundamental insights, our approach can be combined with gene expression studies of various NTRs to understand the cellular response to treatment with NLS-modified agents. Thus, aspects such as agent concentrations and incubation time points can be further refined in order to delineate the most accurate transport network for a given agent. This method can be further exploited to select specific NLS sequences for particular NTRs. Lastly, an advantage of our current methodology is that these measurements can be made in a structured manner using *in vitro* biochemical methods and can be combined with a proteomic system that can be easily applied to any NLS-modified agent.

MATERIALS AND METHODS

Cell Culture

SKBR3, MCF7, and BT474 cells were obtained from ATCC and were tested for authenticity and contamination with viruses or mycoplasma prior to experimentation. Cells were grown in accordance with ATCC recommendations.

Accum Conjugation and Determination of Accum Loading

Accum was synthesized as previously described.[16] T-DM1 was obtained from the CHUS (Centre Hospitalier Universitaire de Sherbrooke) Pharmacy. The $SM(PEG)_2$ was reacted in molar excess to 200 μg of T-DM1 in order to obtain approximately different amounts of Accum moieties per T-DM1. Reaction conditions to control the amount of Accum per mAb have been previously described.[86] Accum-modified T-DM1 was then transferred to a Centricon YM-100 ultrafiltration tube (EMD Millipore, Etobicoke, ON, Canada) and concentrated in PBS (pH 7.4). Bicinchoninic acid, UV absorbance, and Bradford assays were performed to determine protein concentration.

To determine Accum loading, 10 μg of T-DM1 and Accum-T-DM1 ADCs were loaded onto a 12% polyacrylamide gel. Conjugates were analyzed by SDS-PAGE under reducing conditions on a 12% Tris-HCl polyacrylamide gel and stained with Coomassie brilliant blue R-250 (Bio-Rad, Mississauga, ON, Canada). The migration distance in the gel relative to the blue dye front (Rf) was measured and the numbers of Accum moieties introduced into the LC and HC of T-DM1 were categorized into low, medium, and high Accum loads estimated by reference to a logarithm plot of molecular weight versus 1/Rf for Kaleidoscope prestained standards (Bio-Rad) electrophoresed under identical conditions. Similar procedures were performed for Accum modification of Tmab, or NLS (no cholic acid) modification of T-DM1.

Turbidity and Differential Scanning Fluorimetry

Turbidity assays were performed after the purification and concentration steps. T-DM1 or Accum-T-DM1 suspended in 100 μL of PBS was loaded into 96-well quartz plates and analyzed at the visible wavelength of 560 nm. The amount of blocked wavelength directly correlated with increase turbidity of the solution.

For differential scanning fluorimetry, lyophilized T-DM1 was suspended in PBS and the Accum-T-DM1 formulations were evaluated from solution obtained after concentration. 10 μL of 1 mg/mL ADCs was loaded into standard capillaries and mounted in a Prometheus NT.48 (NanoTemper Technologies, Germany) with excitation near UV. The temperature gradient was set to 1°C/min in the range of 20°C–95°C. ADC unfolding was measured by detecting the change in tryptophan/tyrosine fluorescence at emission wavelengths of 330 and 350 nm as a function of temperature. Melting temperatures were determined by detecting the maximum of the first derivative of the fluorescence ratios (350 nm/330 nm). Raw data were analyzed using ThermControl software, and statistics were calculated using Excel.

Flow Cytometry

1×10^6 SKBR3 cells were seeded in six-well plates 24 h prior to experimentation. Cells were washed once with PBS and then treated with 7.5 μg/mL of conjugates in media for 15 min, 30 min, 1 h, 2 h, 4 h, 6 h, and 8 h. At the end of each indicated time at 37°C, cells were lifted with 250 μL of 0.25% trypsin/ETDA (Wisent) for 5 min at room temperature (RT), suspended in 1 mL of complete media, and centrifuged for 5 min at 1,000 × *g*. Supernatant was removed and cells were washed twice with ice-cold PBS. Washed cells were then fixed in 1% paraformaldehyde (PFA) and 1% sucrose in PBS for 30 min on ice. Fixed cells were then washed twice with PBS and permeabilized using 0.015% Triton X-100 in PBS for 10 min at RT. Cells were then incubated in rabbit anti-human IgG conjugated to Alexa Fluor 647 (Invitrogen) for 1 h, on ice, in the dark, and washed twice in PBS. 10 μg/mL of PI was then added to the tubes. Fluorescence was measured on a CytoFLEX 15 (Beckman Coulter), and 10,000 cells per sample were analyzed. Data were analyzed using CytExpert (version 2.0, Beckman Coulter).

Immunofluorescence Confocal Microscopy

SKBR3 cells in media were treated with 7.5 μg/mL of Accum-T-DM1 and T-DM1 for up to 2 h at 37°C. Cells were fixed using 4% PFA and 4% sucrose in PBS at 4°C for 30 min, and permeabilized with 0.1% Triton X-100 in PBS for 15 min at RT. Subsequent steps were made in the blocking buffer containing 10% bovine serum albumin in PBS. Blocking was performed for 30 min at RT and incubation with rabbit anti-human Alexa Fluor 647 (Invitrogen) that binds to the Tmab Fc region of T-DM1 and Accum-T-DM1. Nuclear staining was performed with Hoechst (1:10,000) concurrently for 1 h at RT. Cells were washed and processed, and images were acquired as described.[16]

For the IPO7 knockdown experiments, the Tmab antibody was detected using a primary monoclonal mouse anti-human Fc and secondary polyclonal goat anti-mouse Alexa Fluor 647 (Invitrogen). IPO7 was detected using a primary polyclonal rabbit antibody and secondary polyclonal goat anti-rabbit Alexa Fluor 488 (Invitrogen).

Cytotoxicity Assays

5×10^3 SKBR3 (normal and knocked down) cells in 96-well flat-bottom plates were exposed to increasing concentrations of T-DM1 and

Accum-T-DM1 at 37°C for 72 h. Media were removed and cells were incubated with PrestoBlue (Thermo Fisher) for 30 min and measured in a fluorometric plate reader in accordance with the manufacturer's protocol. Assays were performed in triplicate. Cytotoxicity data were analyzed using nonlinear regression in GraphPad Prism version 7.0

SKBR3 Cell Treatment and Affinity Purification

15×10^6 SKBR3 cells were seeded in a 150-mm dish 24 h prior to experimentation. Cells were treated with 7.5 μg/mL of Tmab, T-DM1, or Acc_L-T-DM1 for 2 h at 37°C. Cells were then washed twice with PBS at RT and then lysed with ice-cold radioimmunoprecipitation assay (RIPA) buffer (50 mM Tris-HCl [pH 7.5] at 25°C, 150 mM NaCl, 1% v/v Triton X-100, 0.5% w/v sodium deoxycholate, 1 mM PMSF, 5 mM NaF). Lysates were passed 10 times through a 21-gauge needle and tubes were centrifuged at 20,000 × *g* for 5 min to pellet-insoluble cell debris. Supernatants were transferred to fresh tubes and diluted at a 1:1 ratio in RIPA buffer. 25 μL of protein G-coated magnetic beads (Thermo Fisher Scientific, 10003D) were equilibrated by washing twice in RIPA buffer and then mixed with 1.5 mL of diluted cell lysate for 1 h at RT with inversion. Beads were isolated on a magnetic rack and washed four times in PBS. The pulled down proteins were then processed for HPLC-MS/MS analysis or western blot.

Sample Preparation for HPLC-MS/MS

Beads from pull-downs were transferred to fresh tubes and washed five times with 20 mM NH_4HCO_3 in MS-grade water. After the final wash, the beads were suspended in 100 μL of NH_4HCO_3 buffer containing 10 mM dithiothreitol (DTT) and incubated at 60°C with mixing for 30 min. Tubes were cooled to RT and 15 mM iodoacetamide was added and incubated for an additional 1 h at RT in the dark with mixing. The iodoacetamide was then quenched by the addition of 1 M DTT to a final concentration of 15 mM DTT and left for 10 min.

On-bead digestion was performed by adding 1 μg of MS-grade trypsin (Promega, V5280) to each tube and incubating at 37°C with shaking at 350 rpm overnight. The following day, MS-grade formic acid (FA) up to 1% final concentration was added to quench digestion. Tubes were set on a magnetic rack to pellet the beads, and the supernatant containing the peptides was transferred to fresh tubes. The beads were then washed in 100 μL of 60% MS-grade acetonitrile in 0.1% FA for 5 min. The supernatants were then pooled and then dried under vacuum. Peptide desalting and HPLC-MS/MS were performed using the identical methods and parameters as described by Chauvin and Boisvert.[87] The sample preparation and HPLC-MS/MS were performed five independent times using freshly obtained T-DM1 and prepared Accum-T-DM1. The MS proteomics data have been deposited to the ProteomeXchange Consortium via the PRIDE partner repository[88] with the dataset identifier PXD014786.

Label-Free Quantification Data Analysis

MS raw files from the performed HPLC-MS/MS were analyzed with MaxQuant software (version 1.6.0.1). Specificity was set to trypsin, defined as cleavage after a lysine or an arginine not before a proline, maximum of two missed cleavages allowed, and peptides had to be at least 7 aa long. Variable amino acid modification included methionine oxidation and protein N-terminal acetylation. Fixed modification included cysteine carbamidomethylation. The mass tolerance for precursor and fragment ions was 7 and 20 ppm, respectively. Spectra were searched against the UniprotKB (*Homo sapiens*, November 12, 2018, 88,354 entries)[89] for protein identification with a BFDR of 1%. Potential contaminants, reverse peptides, proteins only identified by sites, with less than two unique peptides, and duplicated proteins in the data matrix were excluded. The three replicates that exhibited the most internal reproducibility, to avoid artificial enrichment or impoverishment due to variation in sample processing, were selected for further analysis. The resulting protein groups can be found in Table S1.

SAINT Identification of Accum-Specific Interactors

Spectral counts obtained from MaxQuant were imputed into CRAPome. SAINT analysis was performed on the I:III model using STSc threshold values set at ≥ 0.9 and ≥ 0.5, respectively. The I:I:I:I model was also analyzed by SAINT with a STSc cutoff of 0.9 and included CRAPome controls (CC405, CC406, and CC410).[90] SAINT parameters are available in Tables S2 and S3 for the I:III and I:I:I:I models, respectively.

Network Visualization and GSEA

For the I:III model, a gene list was extracted from the SAINT analysis using STSc ≥ 0.5 and entered into GM (version 3.5.0)[91] in Cytoscape (version 3.6.1). The STSCs were then input into Cytoscape. GSEA was performed by GM to determine the most enriched GO terms. These GO terms were then used to systematically attribute a "generic pathway" to each protein in the network according to their main function. Proteins for which a generic pathway could not be attributed through GM were manually searched in the UniProt Knowledgebase,[89] the Human Protein Atlas,[92–94] and PubMed and assigned to their most significant function. The GM parameters, results, and generic pathway annotations can be found in Table S2. GO terms and q values are listed in Table S4.

For the I:I:I:I model, genes obtained from the SAINT analysis with an STSc ≥ 0.9 were input into GM. The GSEA results were extracted and common pathways were assessed using the Bioinformatics & Evolutionary Genomics tool to generate a Venn diagram (http://bioinformatics.psb.ugent.be/webtools/Venn/). q values obtained from GM were transformed for the purpose of visualization with the following equation: log(1/q value). The I:I:I:I model was used to validate the findings from the I:III model, and thus generic pathways were only assigned to individual genes using GM analysis results and are shown in Table S3. The list of GO terms and enrichment values for the baits are listed in Table S5.

The dot plot was generated using ProHits-viz, an online data visualization too.[95] SAINT results from the I:I:I:I analysis were

imported into the dot plot generator with the following parameters: average spectral count was used for abundance for STSc for confidence scoring, with 0.9 as the primary filter and 0.8 as the secondary filter.

Gene Silencing

siRNAs (pool of four) directed against the indicated genes were obtained from Dharmacon (ON-TARGET plus human KPNA2, #L-004702-00-0005; KPNB1, #L-017523-00-0005; IPO4, #L-009516-01-0005; IPO7, #L-012255-00-0005). For example, 3.5×10^5 cells were transfected according to the manufacturer's protocol using 2 μL of DharmaFECT and 10 μL of 5 μM siRNA pool for 24 h in serum-free medium (Life Technologies) in six-well plates. The cells were then split for cytotoxicity assays and western blot analysis. Transfections were performed in triplicate for each condition. Cytotoxicity assays for gene-silenced cells were performed as previously described.

Western Blot

Western blot was performed to evaluate the MS-identified NTR interactors and to determine NTR gene knockdown. After washing in PBS, the beads were suspended in 50 μL of 2× loading buffer (100 mM Tris-HCl [pH 6.8], 2% SDS, 12% glycerol, 10 mM DTT, and 0.02% bromophenol blue) and boiled for 5 min. Beads were captured on a magnetic support, and 25 μL of supernatant was loaded onto an 8% SDS gel and electrophoresed for 2 h at 150 V. The bicinchoninic acid assay (Bio-Rad) was used to measure protein concentration from the cell lysates, and 20 μg of protein was loaded onto 8% SDS gels and electrophoresed. Proteins were then transferred to a polyvinylidene fluoride [PVDF] membrane overnight, at 4°C under a constant current of 40 mA on ice. PVDF membranes were then rinsed three times in H_2O, dried to fix proteins in place, rehydrated in 100% methanol, washed twice in PBS, washed twice in 50 mM Tris-HCl (pH 7.5), 150 mM NaCl, and 0.1% v/v Tween 20 (TBST), and blocked for 1 h in 5% fat-free milk in TBST with gentle shaking. Membranes were then washed three times with TBST and incubated with mouse polyclonal anti-IPO7 (1:200), rabbit polyclonal anti-IPO4 (1:400), rabbit anti-KPNB1 (1:400), or goat polyclonal anti-KPNA2 (1:500). The mouse polyclonal anti-tubulin (1:500) was used for loading controls. Anti-IPO7, IPO4, and KPNB1 antibodies were purchased from LifeSpan Biosciences. Anti-KPNA2 and tubulin antibodies were purchased from Invitrogen. Incubations were performed at 4°C, in 2.5% milk in TBST, with gentle shaking overnight. Membranes were then washed in TBST three times and incubated for 1 h at RT in 2.5% milk in TBST with horseradish peroxidase (HRP)-conjugated goat anti-rabbit (1:4,000), goat anti-mouse (1:5,000) (Invitrogen), or donkey anti-goat (1:5,000) (Cedarlane). Finally, blots were washed twice with TBST, twice with PBS, and revealed by electrochemiluminescence (Thermo Fisher Scientific).

Modeling

PDB: 6N88 was used to evaluate potential IPO7:Accum-T-DM1 interactions (PyMOL; Schrödinger, New York, NY, USA).

Statistical Analysis

Turbidity for each group was reported as mean ± standard deviation and significance ($p < 0.05$) determined using a 1-way ANOVA with Turkey's multiple comparisons test in GraphPad.

SUPPLEMENTAL INFORMATION

Supplemental Information can be found online at https://doi.org/10.1016/j.omtm.2020.08.016.

AUTHOR CONTRIBUTIONS

V.L. conceived and designed the study, prepared and characterized ADCs, designed the proteomic approach, performed all experiments, and co-wrote the manuscript. S.B performed ADC conjugations and confocal microscopy. S.J. helped conceptualize experiments and interpret data. J.V.L. conceptualized the study, performed modeling analyses, directed the overall approach, and co-wrote the manuscript.

CONFLICTS OF INTEREST

The authors declare no competing interests.

ACKNOWLEDGMENTS

This work was supported by funds from the Canadian Institutes of Health Research (Grant no. 201610PJT-378389-PJT-CFDA-190713) and by Fonds de Recherche Quebec—Santé (FRQS). Thank you to the proteomic platform at the FMSS. S.J. and J.V.L are members of the FRQS-funded Centre de Recherche du CHUS. S.J. and J.V.L also hold faculty salary awards from FRQS. We thank Dr. M. Badr for discussions about stability data. We also thank Dr. D. Levy (University of Wyoming) for thoughtful discussions and comments on the manuscript.

REFERENCES

1. Walsh, G. (2018). Biopharmaceutical benchmarks 2018. Nat. Biotechnol. *36*, 1136–1145.
2. Leyton, J.V. (2020). Improving receptor-mediated intracellular access and accumulation of antibody therapeutics—the tale of HER2. Antibodies (Basel) *9*, E32.
3. Wilson, A.W., and Neumann, P.J. (2012). The cost-effectiveness of biopharmaceuticals: a look at the evidence. MAbs *4*, 281–288.
4. Hobernik, D., and Bros, M. (2018). DNA vaccines-how far from clinical use? Int. J. Mol. Sci. *19*, E3605.
5. Bavelaar, B.M., Lee, B.Q., Gill, M.R., Falzone, N., and Vallis, K.A. (2018). Subcellular targeting of theranostic radionuclides. Front. Pharmacol. *9*, 996.
6. Munsell, E.V., Ross, N.L., and Sullivan, M.O. (2016). Journey to the center of the cell: current nanocarrier design strategies targeting biopharmaceuticals to the cytoplasm and nucleus. Curr. Pharm. Des. *22*, 1227–1244.
7. Slastnikova, T.A., Ulasov, A.V., Rosenkranz, A.A., and Sobolev, A.S. (2018). Targeted intracellular delivery of antibodies: the state of the art. Front. Pharmacol. *9*, 1208.
8. Green, M., Ishino, M., and Loewenstein, P.M. (1989). Mutational analysis of HIV-1 Tat minimal domain peptides: identification of *trans*-dominant mutants that suppress HIV-LTR-driven gene expression. Cell *58*, 215–223.
9. Dinca, A., Chien, W.M., and Chin, M.T. (2016). Intracellular delivery of proteins with cell-penetrating peptides for therapeutic uses in human disease. Int. J. Mol. Sci. *17*, 263.
10. Benavent Acero, F.R., Perera Negrin, Y., Alonso, D.F., Perea, S.E., Gomez, D.E., and Farina, H.G. (2014). Mechanisms of cellular uptake, intracellular transportation, and degradation of CIGB-300, a Tat-conjugated peptide, in tumor cell lines. Mol. Pharm. *11*, 1798–1807.

11. Fischer, R., Bächle, D., Fotin-Mleczek, M., Jung, G., Kalbacher, H., and Brock, R. (2006). A targeted protease substrate for a quantitative determination of protease activities in the endolysosomal pathway. ChemBioChem *7*, 1428–1434.

12. Richard, J.P., Melikov, K., Vives, E., Ramos, C., Verbeure, B., Gait, M.J., Chernomordik, L.V., and Lebleu, B. (2003). Cell-penetrating peptides. A reevaluation of the mechanism of cellular uptake. J. Biol. Chem. *278*, 585–590.

13. Hu, M., Chen, P., Wang, J., Scollard, D.A., Vallis, K.A., and Reilly, R.M. (2007). ^{123}I-labeled HIV-1 tat peptide radioimmunoconjugates are imported into the nucleus of human breast cancer cells and functionally interact in vitro and in vivo with the cyclin-dependent kinase inhibitor, p21$^{WAF-1/Cip-1}$. Eur. J. Nucl. Med. Mol. Imaging *34*, 368–377.

14. Niesner, U., Halin, C., Lozzi, L., Günthert, M., Neri, P., Wunderli-Allenspach, H., Zardi, L., and Neri, D. (2002). Quantitation of the tumor-targeting properties of antibody fragments conjugated to cell-permeating HIV-1 TAT peptides. Bioconjug. Chem. *13*, 729–736.

15. Warso, M.A., Richards, J.M., Mehta, D., Christov, K., Schaeffer, C., Rae Bressler, L., Yamada, T., Majumdar, D., Kennedy, S.A., Beattie, C.W., and Das Gupta, T.K. (2013). A first-in-class, first-in-human, phase I trial of p28, a non-HDM2-mediated peptide inhibitor of p53 ubiquitination in patients with advanced solid tumours. Br. J. Cancer *108*, 1061–1070.

16. Beaudoin, S., Rondeau, A., Martel, O., Bonin, M.A., van Lier, J.E., and Leyton, J.V. (2016). ChAcNLS, a novel modification to antibody-conjugates permitting target cell-specific endosomal escape, localization to the nucleus, and enhanced total intracellular accumulation. Mol. Pharm. *13*, 1915–1926.

17. Paquette, M., Beaudoin, S., Tremblay, M.A., Jean, S., Lopez, A.F., Lecomte, R., Guérin, B., Bentourkia, M., Sabbagh, R., and Leyton, J.V. (2018). NLS-cholic acid conjugation to IL-5Rα-specific antibody improves cellular accumulation and in vivo tumor-targeting properties in a bladder cancer model. Bioconjug. Chem. *29*, 1352–1363.

18. Shivanna, V., Kim, Y., and Chang, K.O. (2014). The crucial role of bile acids in the entry of porcine enteric calicivirus. Virology *456–457*, 268–278.

19. Shivanna, V., Kim, Y., and Chang, K.O. (2015). Ceramide formation mediated by acid sphingomyelinase facilitates endosomal escape of caliciviruses. Virology *483*, 218–228.

20. Contreras, F.X., Villar, A.V., Alonso, A., and Goñi, F.M. (2009). Ceramide-induced transbilayer (flip-flop) lipid movement in membranes. Methods Mol. Biol. *462*, 155–165.

21. Samanta, S., Stiban, J., Maugel, T.K., and Colombini, M. (2011). Visualization of ceramide channels by transmission electron microscopy. Biochim. Biophys. Acta *1808*, 1196–1201.

22. Paquette, M., Vilera-Perez, L.G., Beaudoin, S., Ekindi-Ndongo, N., Boudreaut, P.L., Bonin, M.A., Battista, M.C., Bentourkia, M., Lopez, A.F., Lecomte, R., et al. (2017). Targeting IL-5Rα with antibody-conjugates reveals a strategy for imaging and therapy for invasive bladder cancer. OncoImmunology *6*, e1331195.

23. Fried, H., and Kutay, U. (2003). Nucleocytoplasmic transport: taking an inventory. Cell. Mol. Life Sci. *60*, 1659–1688.

24. Macara, I.G. (2001). Transport into and out of the nucleus. Microbiol. Mol. Biol. Rev. *65*, 570–594.

25. Adam, S.A., and Gerace, L. (1991). Cytosolic proteins that specifically bind nuclear location signals are receptors for nuclear import. Cell *66*, 837–847.

26. Görlich, D., and Kutay, U. (1999). Transport between the cell nucleus and the cytoplasm. Annu. Rev. Cell Dev. Biol. *15*, 607–660.

27. Kalderon, D., Roberts, B.L., Richardson, W.D., and Smith, A.E. (1984). A short amino acid sequence able to specify nuclear location. Cell *39*, 499–509.

28. Lanford, R.E., and Butel, J.S. (1984). Construction and characterization of an SV40 mutant defective in nuclear transport of T antigen. Cell *37*, 801–813.

29. Christie, M., Chang, C.W., Róna, G., Smith, K.M., Stewart, A.G., Takeda, A.A., Fontes, M.R., Stewart, M., Vértessy, B.G., Forwood, J.K., and Kobe, B. (2016). Structural biology and regulation of protein import into the nucleus. J. Mol. Biol. *428* (10 Pt A), 2060–2090.

30. Escriou, V., Carrière, M., Scherman, D., and Wils, P. (2003). NLS bioconjugates for targeting therapeutic genes to the nucleus. Adv. Drug Deliv. Rev. *55*, 295–306.

31. Pichon, C., Billiet, L., and Midoux, P. (2010). Chemical vectors for gene delivery: uptake and intracellular trafficking. Curr. Opin. Biotechnol. *21*, 640–645.

32. Pouton, C.W., Wagstaff, K.M., Roth, D.M., Moseley, G.W., and Jans, D.A. (2007). Targeted delivery to the nucleus. Adv. Drug Deliv. Rev. *59*, 698–717.

33. Sun, Y., Xian, L., Xing, H., Yu, J., Yang, Z., Yang, T., Yang, L., and Ding, P. (2016). Factors influencing the nuclear targeting ability of nuclear localization signals. J. Drug Target. *24*, 927–933.

34. Won, Y.W., Lim, K.S., and Kim, Y.H. (2011). Intracellular organelle-targeted non-viral gene delivery systems. J. Control. Release *152*, 99–109.

35. Chook, Y.M., and Süel, K.E. (2011). Nuclear import by karyopherin-βs: recognition and inhibition. Biochim. Biophys. Acta *1813*, 1593–1606.

36. Baade, I., and Kehlenbach, R.H. (2019). The cargo spectrum of nuclear transport receptors. Curr. Opin. Cell Biol. *58*, 1–7.

37. Jäkel, S., and Görlich, D. (1998). Importin β, transportin, RanBP5 and RanBP7 mediate nuclear import of ribosomal proteins in mammalian cells. EMBO J. *17*, 4491–4502.

38. Mosammaparast, N., Jackson, K.R., Guo, Y., Brame, C.J., Shabanowitz, J., Hunt, D.F., and Pemberton, L.F. (2001). Nuclear import of histone H2A and H2B is mediated by a network of karyopherins. J. Cell Biol. *153*, 251–262.

39. Mühlhäusser, P., Müller, E.C., Otto, A., and Kutay, U. (2001). Multiple pathways contribute to nuclear import of core histones. EMBO Rep. *2*, 690–696.

40. Verma, S., Miles, D., Gianni, L., Krop, I.E., Welslau, M., Baselga, J., Pegram, M., Oh, D.Y., Diéras, V., Guardino, E., et al.; EMILIA Study Group (2012). Trastuzumab emtansine for HER2-positive advanced breast cancer. N. Engl. J. Med. *367*, 1783–1791.

41. Sung, M., Tan, X., Lu, B., Golas, J., Hosselet, C., Wang, F., Tylaska, L., King, L., Zhou, D., Dushin, R., et al. (2018). Caveolae-mediated endocytosis as a novel mechanism of resistance to trastuzumab emtansine (T-DM1). Mol. Cancer Ther. *17*, 243–253.

42. Austin, C.D., De Mazière, A.M., Pisacane, P.I., van Dijk, S.M., Eigenbrot, C., Sliwkowski, M.X., Klumperman, J., and Scheller, R.H. (2004). Endocytosis and sorting of ErbB2 and the site of action of cancer therapeutics trastuzumab and geldanamycin. Mol. Biol. Cell *15*, 5268–5282.

43. Oroudjev, E., Lopus, M., Wilson, L., Audette, C., Provenzano, C., Erickson, H., Kovtun, Y., Chari, R., and Jordan, M.A. (2010). Maytansinoid-antibody conjugates induce mitotic arrest by suppressing microtubule dynamic instability. Mol. Cancer Ther. *9*, 2700–2713.

44. Hommelgaard, A.M., Lerdrup, M., and van Deurs, B. (2004). Association with membrane protrusions makes ErbB2 an internalization-resistant receptor. Mol. Biol. Cell *15*, 1557–1567.

45. Longva, K.E., Pedersen, N.M., Haslekås, C., Stang, E., and Madshus, I.H. (2005). Herceptin-induced inhibition of ErbB2 signaling involves reduced phosphorylation of Akt but not endocytic down-regulation of ErbB2. Int. J. Cancer *116*, 359–367.

46. Kim, M.T., Chen, Y., Marhoul, J., and Jacobson, F. (2014). Statistical modeling of the drug load distribution on trastuzumab emtansine (Kadcyla), a lysine-linked antibody drug conjugate. Bioconjug. Chem. *25*, 1223–1232.

47. Wakankar, A.A., Feeney, M.B., Rivera, J., Chen, Y., Kim, M., Sharma, V.K., and Wang, Y.J. (2010). Physicochemical stability of the antibody-drug conjugate trastuzumab-DM1: changes due to modification and conjugation processes. Bioconjug. Chem. *21*, 1588–1595.

48. Cilliers, C., Menezes, B., Nessler, I., Linderman, J., and Thurber, G.M. (2018). Improved tumor penetration and single-cell targeting of antibody-drug conjugates increases anticancer efficacy and host survival. Cancer Res. *78*, 758–768.

49. Buecheler, J.W., Winzer, M., Tonillo, J., Weber, C., and Gieseler, H. (2018). Impact of payload hydrophobicity on the stability of antibody-drug conjugates. Mol. Pharm. *15*, 2656–2664.

50. Luo, Q., Chung, H.H., Borths, C., Janson, M., Wen, J., Joubert, M.K., and Wypych, J. (2016). Structural characterization of a monoclonal antibody-maytansinoid immunoconjugate. Anal. Chem. *88*, 695–702.

51. Erickson, H.K., Lewis Phillips, G.D., Leipold, D.D., Provenzano, C.A., Mai, E., Johnson, H.A., Gunter, B., Audette, C.A., Gupta, M., Pinkas, J., and Tibbitts, J.

(2012). The effect of different linkers on target cell catabolism and pharmacokinetics/pharmacodynamics of trastuzumab maytansinoid conjugates. Mol. Cancer Ther. *11*, 1133–1142.

52. Lewis Phillips, G.D., Li, G., Dugger, D.L., Crocker, L.M., Parsons, K.L., Mai, E., Blättler, W.A., Lambert, J.M., Chari, R.V., Lutz, R.J., et al. (2008). Targeting HER2-positive breast cancer with trastuzumab-DM1, an antibody-cytotoxic drug conjugate. Cancer Res. *68*, 9280–9290.

53. Junttila, T.T., Li, G., Parsons, K., Phillips, G.L., and Sliwkowski, M.X. (2011). Trastuzumab-DM1 (T-DM1) retains all the mechanisms of action of trastuzumab and efficiently inhibits growth of lapatinib insensitive breast cancer. Breast Cancer Res. Treat. *128*, 347–356.

54. Onsum, M.D., Geretti, E., Paragas, V., Kudla, A.J., Moulis, S.P., Luus, L., Wickham, T.J., McDonagh, C.F., MacBeath, G., and Hendriks, B.S. (2013). Single-cell quantitative HER2 measurement identifies heterogeneity and distinct subgroups within traditionally defined HER2-positive patients. Am. J. Pathol. *183*, 1446–1460.

55. Subik, K., Lee, J.F., Baxter, L., Strzepek, T., Costello, D., Crowley, P., Xing, L., Hung, M.C., Bonfiglio, T., Hicks, D.G., and Tang, P. (2010). The expression patterns of ER, PR, HER2, CK5/6, EGFR, Ki-67 and AR by immunohistochemical analysis in breast cancer cell lines. Breast Cancer (Auckl.) *4*, 35–41.

56. Ram, S., Kim, D., Ober, R.J., and Ward, E.S. (2014). The level of HER2 expression is a predictor of antibody-HER2 trafficking behavior in cancer cells. MAbs *6*, 1211–1219.

57. Lang, W.H., Calloni, G., and Vabulas, R.M. (2018). Polylysine is a proteostasis network-engaging structural determinant. J. Proteome Res. *17*, 1967–1977.

58. Ashburner, M., Ball, C.A., Blake, J.A., Botstein, D., Butler, H., Cherry, J.M., Davis, A.P., Dolinski, K., Dwight, S.S., Eppig, J.T., et al.; The Gene Ontology Consortium (2000). Gene ontology: tool for the unification of biology. Nat. Genet. *25*, 25–29.

59. The Gene Ontology Consortium (2019). The Gene Ontology resource: 20 years and still GOing strong. Nucleic Acids Res. *47* (D1), D330–D338.

60. Sheng, C., Qiu, J., He, Z., Wang, H., Wang, Q., Guo, Z., Zhu, L., and Ni, Q. (2018). Suppression of Kpnβ1 expression inhibits human breast cancer cell proliferation by abrogating nuclear transport of Her2. Oncol. Rep. *39*, 554–564.

61. Andrade, M.A., Petosa, C., O'Donoghue, S.I., Müller, C.W., and Bork, P. (2001). Comparison of ARM and HEAT protein repeats. J. Mol. Biol. *309*, 1–18.

62. Fontes, M.R., Teh, T., Jans, D., Brinkworth, R.I., and Kobe, B. (2003). Structural basis for the specificity of bipartite nuclear localization sequence binding by importin-α. J. Biol. Chem. *278*, 27981–27987.

63. Malik, H.S., Eickbush, T.H., and Goldfarb, D.S. (1997). Evolutionary specialization of the nuclear targeting apparatus. Proc. Natl. Acad. Sci. USA *94*, 13738–13742.

64. Soniat, M., and Chook, Y.M. (2015). Nuclear localization signals for four distinct karyopherin-β nuclear import systems. Biochem. J. *468*, 353–362.

65. Ivic, N., Potocnjak, M., Solis-Mezarino, V., Herzog, F., Bilokapic, S., and Halic, M. (2019). Fuzzy interactions form and shape the histone transport complex. Mol. Cell *73*, 1191–1203.e6.

66. Rix, U., and Superti-Furga, G. (2009). Target profiling of small molecules by chemical proteomics. Nat. Chem. Biol. *5*, 616–624.

67. Liu, W., Chang, J., Liu, M., Yuan, J., Zhang, J., Qin, J., Xia, X., and Wang, Y. (2017). Quantitative proteomics profiling reveals activation of mTOR pathway in trastuzumab resistance. Oncotarget *8*, 45793–45806.

68. Loganzo, F., Tan, X., Sung, M., Jin, G., Myers, J.S., Melamud, E., Wang, F., Diesl, V., Follettie, M.T., Musto, S., et al. (2015). Tumor cells chronically treated with a trastuzumab-maytansinoid antibody-drug conjugate develop varied resistance mechanisms but respond to alternate treatments. Mol. Cancer Ther. *14*, 952–963.

69. Ramello, M.C., Benzaïd, I., Kuenzi, B.M., Lienlaf-Moreno, M., Kandell, W.M., Santiago, D.N., Pabón-Saldaña, M., Darville, L., Fang, B., Rix, U., et al. (2019). An immunoproteomic approach to characterize the CAR interactome and signalosome. Sci. Signal. *12*, eaap9777.

70. Hofmann, D., Tenzer, S., Bannwarth, M.B., Messerschmidt, C., Glaser, S.F., Schild, H., Landfester, K., and Mailänder, V. (2014). Mass spectrometry and imaging analysis of nanoparticle-containing vesicles provide a mechanistic insight into cellular trafficking. ACS Nano *8*, 10077–10088.

71. Yan, Y., Lai, Z.W., Goode, R.J., Cui, J., Bacic, T., Kamphuis, M.M., Nice, E.C., and Caruso, F. (2013). Particles on the move: intracellular trafficking and asymmetric mitotic partitioning of nanoporous polymer particles. ACS Nano *7*, 5558–5567.

72. Park, J.S., Yi, S.W., Kim, H.J., Oh, H.J., Lee, J.S., Go, M., Shim, S.H., and Park, K.H. (2018). Verification of long-term genetic stability of hMSCs during subculture after internalization of sunflower-type nanoparticles (SF-NPs). Theranostics *8*, 5548–5561.

73. Endo, Y., Takeda, K., Mohan, N., Shen, Y., Jiang, J., Rotstein, D., and Wu, W.J. (2018). Payload of T-DM1 binds to cell surface cytoskeleton-associated protein 5 to mediate cytotoxicity of hepatocytes. Oncotarget *9*, 37200–37215.

74. Kim, Y.H., Han, M.E., and Oh, S.O. (2017). The molecular mechanism for nuclear transport and its application. Anat. Cell Biol. *50*, 77–85.

75. Aronsohn, A.I., and Hughes, J.A. (1998). Nuclear localization signal peptides enhance cationic liposome-mediated gene therapy. J. Drug Target. *5*, 163–169.

76. Dominguez-Berrocal, L., Cirri, E., Zhang, X., Andrini, L., Marin, G.H., Lebel-Binay, S., and Rebollo, A. (2019). New therapeutic approach for targeting hippo signalling pathway. Sci. Rep. *9*, 4771.

77. Hébert, E. (2003). Improvement of exogenous DNA nuclear importation by nuclear localization signal-bearing vectors: a promising way for non-viral gene therapy? Biol. Cell *95*, 59–68.

78. Lång, A., Øye, A., Eriksson, J., Rowe, A.D., Lång, E., and Bøe, S.O. (2018). Influence of acute promyelocytic leukemia therapeutic drugs on nuclear pore complex density and integrity. Biochem. Biophys. Res. Commun. *499*, 570–576.

79. Zhang, F., White, R.L., and Neufeld, K.L. (2000). Phosphorylation near nuclear localization signal regulates nuclear import of adenomatous polyposis coli protein. Proc. Natl. Acad. Sci. USA *97*, 12577–12582.

80. Bolhassani, A., Jafarzade, B.S., and Mardani, G. (2017). In vitro and in vivo delivery of therapeutic proteins using cell penetrating peptides. Peptides *87*, 50–63.

81. Efthymiadis, A., Briggs, L.J., and Jans, D.A. (1998). The HIV-1 Tat nuclear localization sequence confers novel nuclear import properties. J. Biol. Chem. *273*, 1623–1628.

82. Kristensen, M., Birch, D., and Mørck Nielsen, H. (2016). Applications and challenges for use of cell-penetrating peptides as delivery vectors for peptide and protein cargos. Int. J. Mol. Sci. *17*, E185.

83. Chuderland, D., Konson, A., and Seger, R. (2008). Identification and characterization of a general nuclear translocation signal in signaling proteins. Mol. Cell *31*, 850–861.

84. Saijou, E., Itoh, T., Kim, K.W., Iemura, S., Natsume, T., and Miyajima, A. (2007). Nucleocytoplasmic shuttling of the zinc finger protein EZI is mediated by importin-7-dependent nuclear import and CRM1-independent export mechanisms. J. Biol. Chem. *282*, 32327–32337.

85. Jäkel, S., Mingot, J.M., Schwarzmaier, P., Hartmann, E., and Görlich, D. (2002). Importins fulfil a dual function as nuclear import receptors and cytoplasmic chaperones for exposed basic domains. EMBO J. *21*, 377–386.

86. Beaudoin, S., Paquette, M., Fafard-Couture, L., Tremblay, M.A., Lecomte, R., Guérin, B., and Leyton, J.V. (2018). Initial evaluation of antibody-conjugates modified with viral-derived peptides for increasing cellular accumulation and improving tumor targeting. J. Vis. Exp. (133), 55440.

87. Chauvin, A., and Boisvert, F.M. (2018). Proteomics analysis of colorectal cancer cells. Methods Mol. Biol. *1765*, 155–166.

88. Perez-Riverol, Y., Csordas, A., Bai, J., Bernal-Llinares, M., Hewapathirana, S., Kundu, D.J., Inuganti, A., Griss, J., Mayer, G., Eisenacher, M., et al. (2019). The PRIDE database and related tools and resources in 2019: improving support for quantification data. Nucleic Acids Res. *47* (D1), D442–D450.

89. The UniProt Consortium (2018). UniProt: the universal protein knowledgebase. Nucleic Acids Res. *46*, 2699.

90. Choi, H., Larsen, B., Lin, Z.Y., Breitkreutz, A., Mellacheruvu, D., Fermin, D., Qin, Z.S., Tyers, M., Gingras, A.C., and Nesvizhskii, A.I. (2011). SAINT: probabilistic scoring of affinity purification-mass spectrometry data. Nat. Methods *8*, 70–73.

91. Montojo, J., Zuberi, K., Rodriguez, H., Kazi, F., Wright, G., Donaldson, S.L., Morris, Q., and Bader, G.D. (2010). GeneMANIA Cytoscape plugin: fast gene function predictions on the desktop. Bioinformatics *26*, 2927–2928.

92. Thul, P.J., Åkesson, L., Wiking, M., Mahdessian, D., Geladaki, A., Ait Blal, H., Alm, T., Asplund, A., Björk, L., Breckels, L.M., et al. (2017). A subcellular map of the human proteome. Science *356*, eaal3321.

93. Uhlén, M., Fagerberg, L., Hallström, B.M., Lindskog, C., Oksvold, P., Mardinoglu, A., Sivertsson, Å., Kampf, C., Sjöstedt, E., Asplund, A., et al. (2015). Tissue-based map of the human proteome. Science *347*, 1260419.

94. Uhlen, M., Zhang, C., Lee, S., Sjöstedt, E., Fagerberg, L., Bidkhori, G., Benfeitas, R., Arif, M., Liu, Z., Edfors, F., et al. (2017). A pathology atlas of the human cancer transcriptome. Science *357*, eaan2507.

95. Knight, J.D.R., Choi, H., Gupta, G.D., Pelletier, L., Raught, B., Nesvizhskii, A.I., and Gingras, A.C. (2017). ProHits-viz: a suite of web tools for visualizing interaction proteomics data. Nat. Methods *14*, 645–646.